Stony Brook University

New Transition Metal Chemistry With Phosphino-Thiol Ligands

A Thesis Presented

by

David Jacob Spritzer

to

The Graduate School
in Partial Fulfillment of the Requirements
for the Degree of

Master of Science

in

Chemistry

Stony Brook University

May 2010

Stony Brook University

The Graduate School

David Jacob Spritzer

We, the thesis committee for the above candidate for the

Master of Science degree, hereby recommend

acceptance of this thesis.

Dr. Michelle Millar - Thesis Advisor
Associate Professor of Chemistry

Dr. Andreas Mayr – Chairperson of Defense
Professor of Chemistry

Dr. Robert Kerber - Third Member
Professor of Chemistry

This thesis is accepted by the Graduate School

Lawrence Martin
Dean of the Graduate School

Abstract of the Thesis

New Transition Metal Chemistry With Phosphino-Thiol Ligands

by

David Jacob Spritzer

Master of Science
in
Chemistry

Stony Brook University

2010

Hydrogenases are a class of enzyme with the unique ability to catalytically reduce or oxidize hydrogen. Due to this ability they have received much attention from chemists who want to harness this power in a controlled setting. This power will allow not only for the mass production of hydrogen but also the potential for the production of cheaper catalysts to be used in fuel cells. The focus of this research is to create different models for the active site of hydrogenase based around the nickel center of the [NiFe] class of hydrogenase. It is believed that this nickel center is responsible for catalytically producing dihydrogen from two protons and two electrons. Currently no model has the ability to perform this at an efficient rate.

This work primarily uses the potentially tridentate *bis*(2-thiophenyl)phenylphosphine ligand, or H_2[PS2], for short. This ligand represents the sulfur rich environment of the nickel with its two thiol functional groups, and has shown prior success in making stable metal complexes at a few different oxidation states. Metal complexes of vanadium, chromium, and manganese containing this ligand were successfully synthesized and characterized using single crystal X-ray diffraction, cyclic voltammetry, and ultraviolet-visible spectroscopy.

Table of Contents

List of Figures

List of Tables

List of Abbreviations

acac: acetylacetone anion

ether: diethyl ether

H_2[PS2]: 2,2'-(phenylphosphinediyl)dibenzenethiol

[PS2]: 2,2'-(phenylphosphinediyl)dibenzenethiolate

H_2[PS2']: 2,2'-(phenylphosphinediyl)bis(4-methylbenzenethiol)

[PS2']: 2,2'-(phenylphosphinediyl)bis(4-methylbenzenethiolate)

H_2[POS2]: 2,2'-(phenylphosphoryl)dibenzenethiol

[POS2]: 2,2'-(phenylphosphoryl)dibenzenethiolate

TMEDA: tetramethylethylenediamine

n-BuLi: n-butyllithium

THF: tetrahydrofuran

PCl_2Ph: phenyldichlorophosphine

$(Et_4N)Br$: tetraethylammonium bromide

$(Pr_4N)Br$: tetrapropylammonium bromide

$(Bu_4N)Br$: tetrabutylammonium bromide

CH_2Cl_2: methylene chloride

$(Fc)BF_4$: ferrocenium tetrafluoroborate

CV: cyclic voltammetry

UV-VIS: ultraviolet-visible

DMF: dimethylformamide

OAc: acetate anion

sh: shoulder

mins: minutes

Acknowledgments

I would like to thank my advisor, Dr. Michelle Millar, for her guidance and support over the past years. Thank you for sharing your knowledge and expertise of chemistry with me. I would also like to thank Dr. Stephen Koch for his help in solving and refining my crystal structures as well as answering my questions related to CV. I must also thank the members of the Millar and Koch labs, Soumya Bhattacharya, Daniel Amarante, Lu Gan, Su'add Zaman, and Anthony Pesiri. You all have been very helpful in my research and great friends.

The chemistry main office staff also deserves thanks. Especially Katherine Hughes, who always went above and beyond her duties to ensure I had everything completed not only for my graduation by during my transition from an undergraduate to a graduate student.

I am thankful for the love and support I have received from my family. My parents, Risa and Shlomo, have always been there for me with endless encouragement and advice. I cannot thank them enough. I would like to thank my sister, Danya, for her constant willingness to listen to me. Finally, I would like to thank my wonderful girlfriend, Mei, for her love and support. You have always been there for me when I needed you and for that I am grateful.

Introduction

Transition metals are widely known to be found at the active site of a large number of biologically significant enzymes. One class of enzyme which has received much attention over the past two decades are the hydrogenases. These enzymes catalyze the reversible oxidation of dihydrogen and the reduction of the hydrogen ions. The basic chemical reaction is expressed as:

$2\,H^+ + 2\,e^- \leftrightarrows H_2$ (1)

This manipulation of hydrogen has made this class of enzyme a topic of much study. One goal of synthesizing hydrogenase models is to create a small metal complex that creates a less energy expensive method of producing hydrogen. Currently, hydrogen is produced by electrochemically splitting water into hydrogen and oxygen. The problem with this method is that more energy is put into the splitting of water than can be generated by using the hydrogen and oxygen that is formed. The electricity needed for this process is usually generated from burning fossil fuels which negates the advantage that hydrogen is a clean source of fuel. By coating the hydrogen producing electrode of this cell with a hydrogenase model, the electricity needed to split the water could be greatly reduced. This could make hydrogen production finally economically feasible[1].

The ultimate goal of these studies is the synthesis of a cheaper catalyst (ideally using the more abundant first row transition metals) than what is currently found in the current fuel cells, which use expensive transition metals such as platinum[2]. Platinum has other limitations besides its expense. It is believed that no new major platinum deposits will be found. Additionally, after a detailed estimation it was found that there is only

enough platinum in the world to sustain automobiles for 15 years (assuming all of the mined platinum went only into manufacturing fuel cells)[3].

Hydrogenase is a useful "starting point" for these models as it already catalytically effects the formation of hydrogen. The most advanced models only are able to catalyze this conversion of hydrogen at higher potentials than the actual enzyme. Ideally a catalyst can be discovered which reduces hydrogen ions to hydrogen at low potentials.

Currently three types of hydrogenases enzymes have been isolated, [Fe] hydrogenase, [FeFe] hydrogenase and [NiFe] hydrogenase. (Figure 1). [Fe] hydrogenases have been shown to contain one iron coordinated to two CO ligands and a cysteine. [FeFe] hydrogenases have been found primarily to reduce protons to dihydrogen. The structure of these enzymes has been found to contain bimetallic iron centers bridged by dithiolates. The iron centers contain several CN^- and CO ligands as well[4]. It is believed that models for this type of hydrogenase would be most useful to assist in hydrogen production by lowering the energy of the process, as mentioned above[1].

The [NiFe] hydrogenases are slightly more mysterious. They are believed to be responsible for the reversible formation and consumption of H_2. Their structures have been also found to contain CN^- and CO ligands on the iron center. The nickel center is in a thiolate rich environment and bridged to the iron center with two cysteinate amino acids. The mechanisms by which these enzymes operate are under constant study and revision. A discussion of the various proposed mechanisms will not be discussed here.

This work is focused on gaining information that will assist us in obtaining novel models for the active site in hydrogenase that will ideally behave similar to the enzyme.

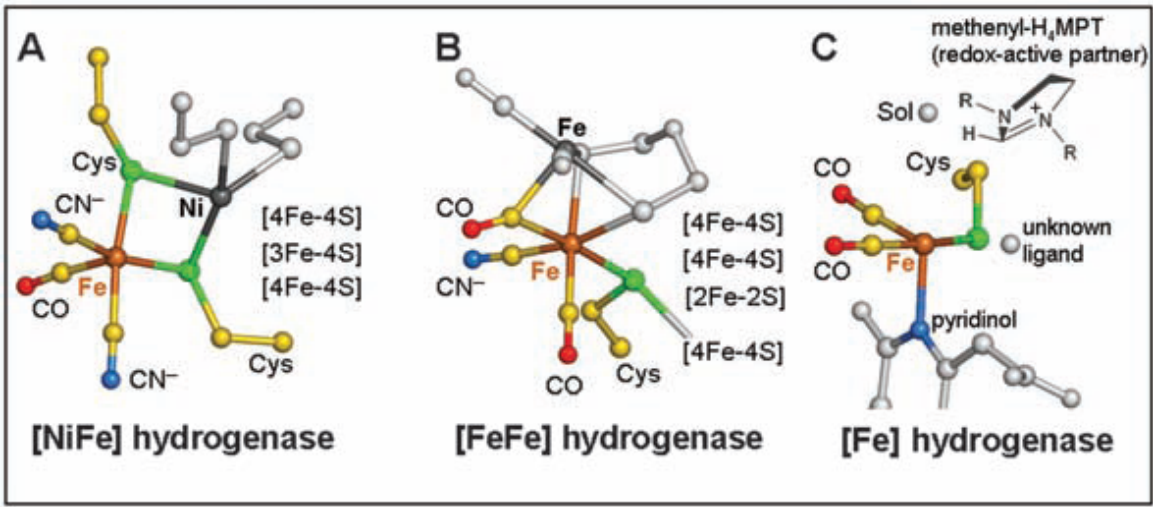

Figure 1: The active sites of different hydrogenases[5].

The goal of this work is to characterize different transition metal complexes with phosphino-thiolate donor ligands. This serves two purposes, first to potentially create a catalyst that can catalyze the formation of H_2, as hydrogenase does. Second to explore the nature of transition metal thiolate centers similar to those which are not only found in hydrogenase but also in a variety of enzymes. This work focuses on exploring the nature of thiolate bonds with transition metals not traditionally found in biological catalysts as these metals have not received much attention in the past. Yet it is important to study these complexes as they could offer insight into how the biological catalysts function.

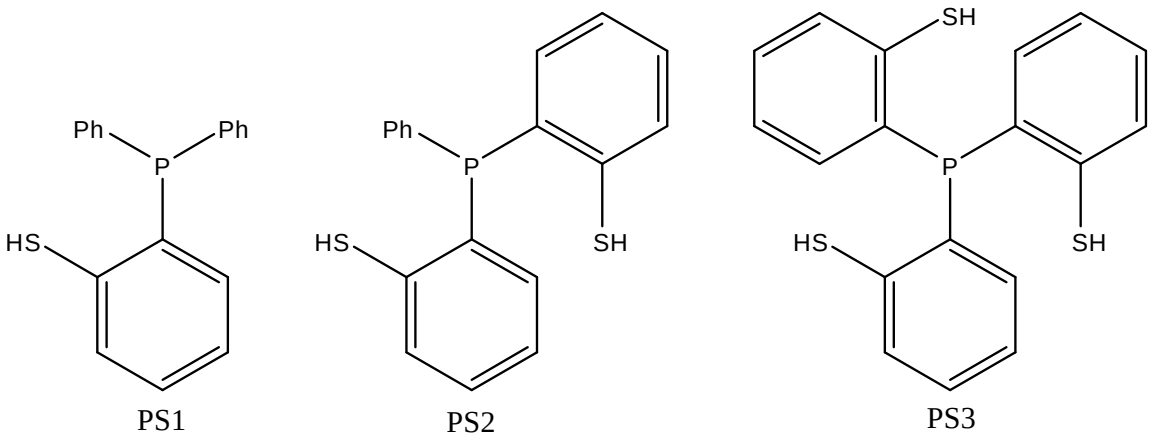

Figure 2a: The family of "PS" ligands.

A variety of phosphorus-thiol containing ligands can be prepared[6] (Figure 2). The ligand used in this work, [PS2] (and the almost chemically identical [PS2'] ligand, with metyl groups *para* to its thiol functional group) were chosen for a variety of reasons. First and foremost this ligand with its two thiolate functional groups mimics the thiolate functional groups found on cysteine in metalloenzymes. The fact that the ligand contains a phosphine binding group and two thiolate binding groups is significant. This allows the ligand to modulate the reactivity of the active site (the metal center). The tridentate properties of this ligand also lend to its usefulness. The reactivity of the metal to undergo certain reactions such as oxidative addition can be studied without having to fear the ligand being completely removed for the metal which would allow for other side reactions such as a ligand substitution. Sulfur itself is known to have rich chemistry with metals. This can be attributed to the lone pairs present on the thiolate ion[7].

Synthetically this type of ligand has certain advantages as well. The fact that the binding functional groups are linked by phenylene bridges allows the ligand to be more

thermally and photochemically stable. It has been observed that ethylene bridged analogues are indeed unstable to photochemical attack via an intermolecular process involving radicals. The H_2[PS2] ligand and its similar analogues (H[PS1] and H_3[PS3]) have not been observed to chemically change after prolonged periods of time. This conclusion has been reached in the literature as well as in the Millar laboratory. This situation allows the H_2[PS2] ligand to be produced on a

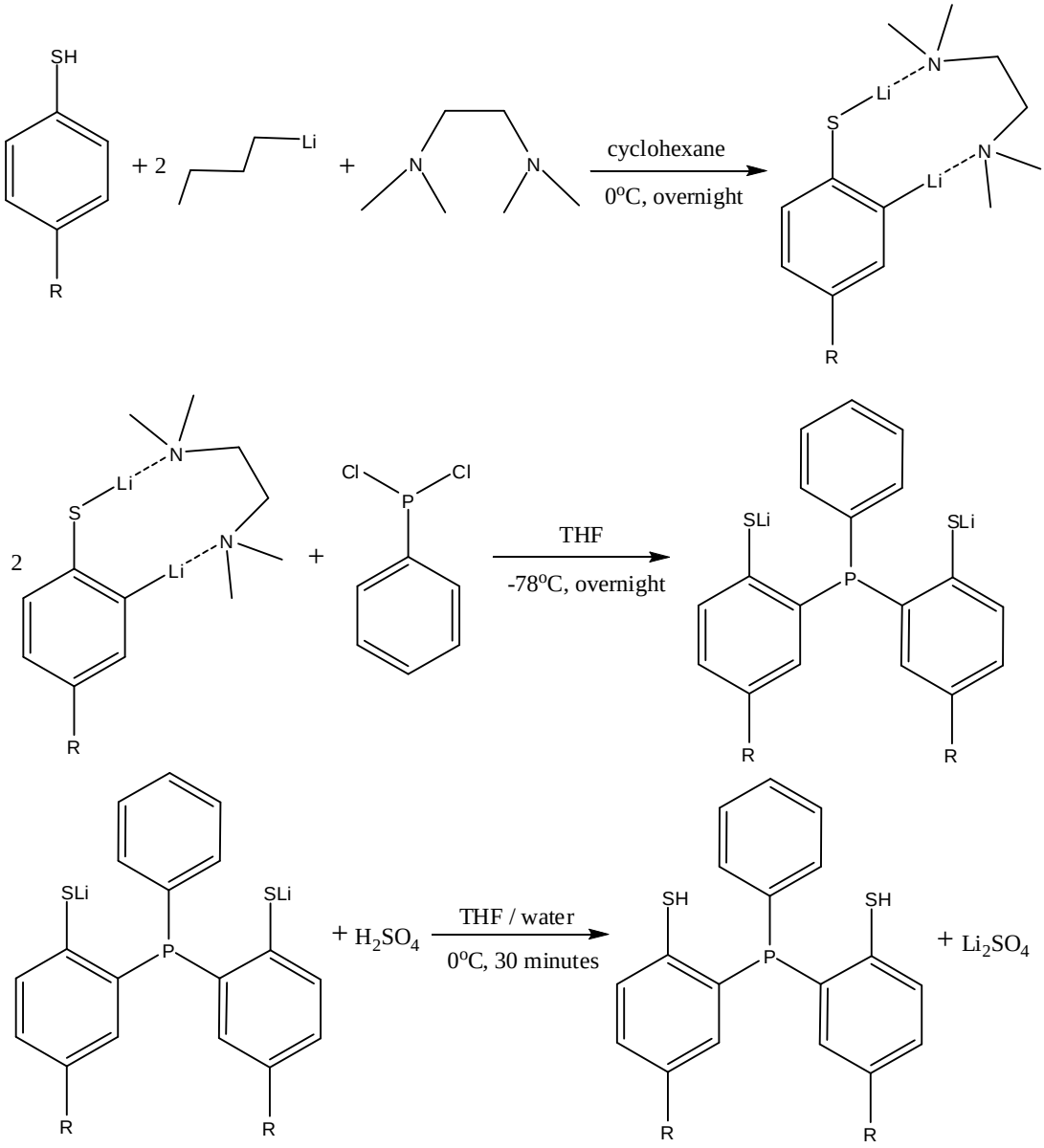

Figure 2b: Synthetic Scheme of H_2[PS2] and H_2[PS2'].

large scale without the need to be concerned about its shelf life. This brings to attention another advantage of this ligand, its ready synthetic preparation (see Synthetic Scheme). The discovery of the ortho-lithiation of benzenethiol allowed for a simple two step reaction to produce a variety of phosphino-thiol ligands[6,8]. Since this discovery there have been a variety of different types of these ligands synthesized and studied. In the laboratory H_2[PS2] can be synthesized within three or four days on scales greater than ten grams and stored indefinitely in a closed container.

Another advantage to using this ligand is the past success of [PS2] in forming stable metal complexes[9]. In these examples, two [PS2] ligands generally bind to one metal center to form a distorted 6-coordinate octahedral geometry. The fact that [PS2] is a tridentate ligand makes these complexes stable. [PS2] also has the ability to form metal complexes with metals in high oxidation states (e.g M(III), and M(IV)). This is useful because then the behavior of these metals at high oxidation states can be studied once the complex is isolated.

There are several examples of crystal structures of PS2 with various transition metals. For example, a $[Mn^{IV}(PS2)_2]$ was synthesized and characterized using X-ray diffraction[10]. A V(IV) compound was also synthesized with a ligand that is chemically similar to [PS2][11]. A $[W^{IV}(PS2)_2]$ was also synthesized and characterized using X-ray diffraction[12]. These complexes will be discussed more in depth below.

Some work has been done in exploring the chemistry of vanadium and molybdenum with [PS2] and [PS3] but in the context of studying the nature of the nitrogenase enzymes, not hydrogenase enzymes. In fact the majority of the literature that is concerned with [PS2] and [PS3] involves complexes of [PS2] and [PS3] with

vanadium[13,14,15] and molybdenum[16]. Nonetheless this work represents advancements in this field and these complexes could also have their uses when studying hydrogenase. Interestingly a seven coordinated vanadium complex was synthesized and its structure determined[17].

Yet there are still many transition metals which for which [PS2] complexes have not been synthesized and studied, particularly metals which are not traditionally associated with having a widespread role in biological systems. Specifically, nickel, and iron have been the focus of many works due to the fact that these metals are present in the hydrogenase enzyme. The goal of this work is to attempt to synthesize and characterize structures of [PS2] with vanadium, chromium, manganese and molybdenum.

The purpose of this study is to have these compounds characterized so that they may be used as a catalyst to generate hydrogen or as a tool that will help scientists understand how the hydrogenase enzyme (particularly the [NiFe] type) catalyzes the production of hydrogen. It is the hope that these compounds will offer an alternative view on designing a model for hydrogenase. Namely, that metals that are less prevalent in biological systems can function just as well, if not better than metals that are more prevalent in biological systems (such as nickel and iron). Further investigation must be done if these complexes are more efficient catalysts. It would be ideal if this were the case along with the possibility that these complexes are cheaper to mass produce and more stable.

Experimental Techniques

General Methods

The syntheses of ligands and metal complexes were carried out under dinitrogen using conventional Schlenk techniques unless otherwise specified. TMEDA, cyclohexane, and THF were all distilled using Na/benzophenone to eliminate any moisture. Methanol was distilled using Mg/I_2 to eliminate any moisture. All other solvents were used as is unless otherwise specified.

Instrumentation

Electrochemistry

Cyclic voltammograms were recorded on a BAS-100W electrochemical analyzer with a platinum working electrode, a platinum wire auxiliary electrode, and a Ag^0/AgCl reference electrode. Samples (ca. 1.0 mM) were measured in the specified solvent with tetra-n-butylammonium tetrafluoroborate (0.10 M) as the supporting electrolyte.

Electronic Spectroscopy (UV-VIS)

UV-VIS spectra were generated using an HP 8453 UV-Visible Spectrophotometer. A tungsten lamp was used for the visible region and a deuterium lamp was used for the ultraviolet region. All samples were scanned using two cells of different path lengths, 0.1 mm and 1.0 mm.

X-ray Diffraction

Cell parameters and data collection summaries for the complexes are given in the tables below. The X-ray crystal data of $[Mn^{IV}(PS2')_2]$ were obtained on a Bruker SMART-1000 single crystal X-ray diffractometer operating at 50 kV and 40 mA, Mo Kα (λ = 0.71073 Å) radiation. The data reduction was done with SAINTPLUS (Bruker); and structure refinement, with SHELXL-97 (Sheldrick). The X-ray crystal data of the other complexes were obtained on an Oxford single crystal X-ray diffractometer operating at 50 kV and 40 mA, Mo Kα (λ = 0.71073 Å) radiation. The structure refinement was done with SHELXL-97 (Sheldrick). All of the crystal structures were solved by direct methods, and anisotropic refinement for all non-hydrogen atoms was done by a full-matrix least-squares method.

Experimental

Synthesis of H_2[PS2]:

The compound was synthesized similarly by literature procedure[6]. A Schlenk flask was charged with 75 mL of freshly distilled cyclohexane, freshly distilled TMEDA [47.0 mL (315 mmol)], and n-BuLi [123 mL (308 mmol)] of 2.5 M in hexanes at 0°C. To a separate Schlenk flask, 15.2 g (138 mmol) of thiophenol was dissolved in 50 mL of freshly distilled cyclohexane. The thiophenol solution was slowly added (drop wise) to the n-BuLi/TMEDA solution at 0°C. The resulting golden yellow solution was left to stir overnight. The next day a white precipitate was observed in the golden yellow solution. The white product was filtered off under nitrogen, washed with 100 mL of distilled cyclohexane, and left to dry *in vacuo*. The reaction yielded 31.0 g of Li_2[PhS] · TMEDA, weighed out in a dry box. This solid was then dissolved in 200 mL of freshly distilled THF and then cooled to -78°C in a dry ice/acetone bath. Dichlorophenylphosphine [8.80 mL (64.8 mmol)] was dissolved in 40 mL of freshly distilled THF in a separate Schlenk flask. This solution was added drop wise to the Li_2[PhS] · TMEDA solution at -78°C. The resulting solution was stirred overnight. The next day the solution had a clear red appearance. 36 mL of a 20% sulfuric acid/distilled water (m/v) and 100 mL of distilled water were added at 0°C to reach a pH of 6 in the organic layer. At this point the solution became a clear golden yellow with some lithium sulfate observed precipitating out. The organic layer was separated from the aqueous layer. The aqueous layer was extracted with 200 mL of diethyl ether and both organic layers were combined. The organic layer was then extracted with 250 mL of a concentrated brine solution. The organic layer was

dried with sodium sulfate for 45 minutes. The drying agent was filtered off and the organic solvents were removed under reduced pressure to give a green-brown oil. This oil was stirred overnight with 50 mL of methanol. The next day the oil was broken up and a white solid appeared. The product was filtered and washed with two portions of 25 mL of methanol. The white product was dried to yield 14.0 g (42.9 mmol, 62.3% yield) of product. The H_2[PS2'] ligand can be synthesized in the same matter using 4-methylthophenol instead of thiophenol.

Synthesis of $V^{III}Cl_3(THF)_3$:

The compound was synthesized by literature procedure[18]. $V^{III}Cl_3$ [5.00 g (31.8 mmol)] was added to 100 mL of freshly distilled THF in a Schlenk flask. The mixture was refluxed for 22 hours. After being cooled to room temperature some pink microcrystals were seen in the solution. Upon being further cooled to -78°C in a dry ice/acetone bath more pink microcrystals were seen. The mixture was filtered, washed once with 30 mL of freshly distilled pentane, and dried *in vacuo*. 8.11 g (21.7 mmol, 68.2% yield) of pink microcrystalline product was afforded.

Synthesis of $Cr^{II}_2(OAc)_4 \cdot 2H_2O$:

The compound was synthesized by literature procedure[19]. To a Schlenk, 25 mL (1:1 v/v) mixture of concentrated HCl and distilled water was added. Chromium metal [4.00 g (77 mmol)] was added to the flask with stirring, which was then degassed. After bubbles of H_2 gas appeared, 20 mL of distilled water was added to the reaction mixture. The reaction mixture was then heated on a steam bath for one hour during which the

mixture turned from a light blue to a dark green-blue color. To a separate Schlenk flask, $NaOAc{\cdot}3H_2O$ [94.0 g (693 mmol)] was added and dissolved in 80 mL of distilled water with gentle heating. The contents of the first reaction flask were then added, drop wise, to the $NaOAc{\cdot}3H_2O$ solution through a frit to ensure that none of the unreacted chromium metal would enter the $NaOAc{\cdot}3H_2O$ solution. After the addition of several drops the solution turned a dark purple color with a dark red precipitate seen. This solution was left to sit overnight. The next day the $Cr^{II}_2(OAc)_4{\cdot}2H_2O$ was filtered through a frit. The product appeared as a dark red powder and the filtrate was an intense blue-purple color. The product was washed three times with a total of 120 mL of cold methanol after which it was dried *in vacuo*. The final product weighed 10.2 g (27.1 mmol, 70.0% yield) of product.

Synthesis of $Mo^{III}Cl_3(THF)_3$:

The compound was synthesized by literature procedure[20]. $Mo^{V}Cl_5$ [3.20 g (11.7 mmol)] and tin powder (30 mesh) [2.90 g (24.4 mmol)] were added to a single Schlenk flask in a dry box. 30 mL of freshly distilled ether was then added and the solution was left to stir. After stirring for 35 minutes an orange precipitate was seen in the dark orange solution. This solution was filtered and the precipitate was transferred to a different Schlenk flask in a dry box. 30 mL of freshly distilled THF was added to this product which was then stirred for 3 hours. After 3 hours the solution became a dark red-brown with a salmon colored precipitate seen. The excess tin was separated from the solution and product by using a 20 gauge cannula to cannula the solution and product to a separate

Schlenk flask. The solution was filtered and the precipitate dried *in vacuo*. The final product appeared salmon colored and weighed 2.13 g (5.09 mmol, 43.5% yield).

Synthesis of $(Fc)BF_4$:

The following reaction was done entirely exposed to air, as described in the literature[21]. Ferrocene [5.00 g (26.9 mmol)] was dissolved in 200 mL of ether in a beaker. In a separate beaker, 1,4-Benzoquinone [5.80 g (53.7 mmol)] was dissolved in 250 mL of ether. Then, 50% fluoroboric acid [13.5 mL (104 mmol)] in water was added to the latter solution. The ferrocene solution was slowly poured into the 1,4-Benzoquinone/fluoroboric acid solution. Immediately a red precipitate was seen. The mixture was allowed to stir for 2 hours. The indigo product was filtered and washed with 3 portions of 50 mL of ether. The reaction yielded 6.65 g (24.4 mmol, 90.7% yield) of product.

Synthesis of $[Et_4N][V^{III}(PS2)_2]$:

H_2[PS2] [0.630 g (1.93 mmol)] and lithium metal [0.030 g (4.32 mmol)] were added to a Schlenk flask. Then, 50 mL of freshly distilled methanol was then added to this flask. The mixture was stirred until all of the solid Li_2[PS2] went into solution. To a separate Schlenk flask $V^{III}Cl_3(THF)_3$ [0.290 g (1.84 mmol)] was added and was then degassed. The Li_2[PS2] solution in methanol was quickly transferred to the awaiting $V^{III}Cl_3(THF)_3$ solid via cannula. Immediately the solution became a dark red color. The mixture was left to stir for approximately three hours. Into a separate Schlenk flask, $(Et_4N)Br$ [0.170 g (0.809 mmol)] was dissolved in 15 mL of freshly distilled methanol.

This solution was added drop wise to the reaction mixture solution via cannula. After about ten minutes some red microcrystalline product was seen emerging from the solution. The mixture was left to sit overnight. The following day, additional red microcrystalline product was observed in a light red solution. This product was filtered and dried *in vacuo* to yield 0.480 g (0.580 mmol, 60.0% yield).

Crystals of $[Et_4N][V^{III}(PS2)_2]$ were grown by layering a solution of $Li[V^{III}(PS2)_2]$ in methanol over a concentrated solution of $(Et_4N)Br$ also dissolved in methanol. Upon standing for two days, large, thick, dark purple plates were formed. The solution was observed to be colorless.

UV-VIS: λ_{max}, nm(ε_m, $M^{-1}cm^{-1}$) = 321 (179000), 345 (sh, 167000), 446 (64700), 544 (51000); 1.0 mM in CH_2Cl_2

Electrochemistry: $E_{1/2}$ (ΔE_P) =

Elapsed time:

2 mins: 385 mV (91 mV) 1.0 mM in DMF vs. Ag/AgCl, oxidation

6 mins: 397 mV (88 mV); 541 mV (81 mV) 1.0 mM in DMF vs. Ag/AgCl, oxidation; oxidation

10 mins: 406 mV (91 mV); 547 mV (80 mV) 1.0 mM in DMF vs. Ag/AgCl, oxidation; oxidation

30 mins: 541 mV (78 mV) 1.0 mM in DMF vs. Ag/AgCl, oxidation

Synthesis of $[V^{IV}(PS2)_2]$:

H_2[PS2] [0.250 g (0.766 mmol)] and $V^{IV}O(acac)_2$ [0.100 g (0.377 mmol)] were each (in separate Schlenk flasks) dissolved in 20 mL of distilled methylene chloride and 35 mL of methanol, respectively. The solution of the $V^{IV}O(acac)_2$ was quickly transferred to the H_2[PS2] solution using a cannula. Immediately the reaction mixture became a dark purple with some microcrystalline $V^{IV}O(acac)_2$ remaining outside of the solution. After overnight stirring, approximately three quarters of the methylene chloride was removed under reduced pressure. At this point some dark purple precipitate was seen in the solution. Then, 25 mL of distilled methanol was added and the reaction was left to stir overnight. The next day more dark purple precipitate was seen in a lightly red colored solution. The product was filtered off and dried open to air to yield 0.15 g (0.187 mmol, 49.6% yield) of product as a purple powder.

Crystals of $[V^{IV}(PS2)_2]$ were grown in a vapor diffusion of CH_2Cl_2/ether. After standing for several days, purple prisms were observed to have been formed on the bottom of the vial.

UV-VIS: λ_{max}, nm(ε_m, $M^{-1}cm^{-1}$) = 265 (749000); 1.0 mM in CH_2Cl_2

Electrochemistry: $E_{1/2}$ (ΔE_P) = 222 mV (96 mV) 1.0 mM in DMF vs. Ag/AgCl, reduction

Synthesis of $[Et_4N][Mn^{III}(PS2')_2]$:

Lithium metal [0.015 g (2.2 mmol)] was placed in a Schlenk flask and dissolved in 35 mL of methanol. To this solution of H_2[PS2'] [0.35 g (0.99 mmol)] was added and

then the solution was degassed. To a separate Schlenk flask, $Mn^{II}Cl_2 \cdot 4H_2O$ [0.099 g (0.50 mmol)] was added and then degassed. Once the Li_2[PS2'] had completely dissolved, this solution was added quickly to the second flask, with rapid stirring. Immediately, the solution turned a dark green. The reaction was left to stir overnight. $(Et_4N)Br$ [0.11 g (0.52 mmol)] was added to a separate flask, dissolved in 15 mL of methanol and then degassed. The counter ion was added slowly (drop wise) to the reaction flask. Immediately, some green precipitate was seen in the solution. The mixture was left to sit overnight. Green microcrystalline product was seen in the solution. The product was filtered and dried *in vacuo* to yielded 0.21 g (0.23 mmol, 47% yield).

Crystals of $[Et_4N][Mn^{III}(PS2)_2]$ were grown in a vapor diffusion of CH_2Cl_2/ether. After standing at room temperature for a few days, small green prism-like crystals were obtained that were suitable for X-ray diffraction.

UV-VIS: λ_{max}, nm(ε_m, $M^{-1}cm^{-1}$) = 292 (664000), 464 (74600); 1.0 mM in CH_2Cl_2

Electrochemistry: $E_{1/2}$ (ΔE_P) = 311 mV (75 mV) 1.0 mM in DMF vs. Ag/AgCl, oxidation

Synthesis of $[Mn^{IV}(PS2')_2]$:

In a Schlenk flask, lithium metal [0.017 g (2.4 mmol)] was dissolved in 30 mL of methanol. To this solution of H_2[PS2'] [0.36 g (1.0 mmol)] was added and the solution was degassed. To a separate Schlenk flask was added $Mn^{II}Cl_2 \cdot 4H_2O$ [0.36 g (1.0 mmol)] and then the flask was degassed. Once the Li_2[PS2'] in the first flask dissolved, the entire

solution was added quickly to the second flask, with stirring. Immediately the solution turned a dark green. After stirring for one half hour, the flask was opened to air. After fifteen minutes purple micro crystals were seen in the solution. The solution was left to stir overnight with only the side arm of the flask opened to the air. One half of the solvent was removed from the solution to ensure the maximum yield. The solution and product were then filtered through a frit and dried *in vacuo*. The final product yield was 0.30 g (0.39 mmol, 78% yield). Crystals suitable for single crystal X-ray diffraction were grown by slowly allowing air into a solution of $[Mn^{III}(PS2')_2]^-$ in methanol.

Crystals of $Mn^{IV}(PS2)_2$ were grown by allowing a solution of $Li[Mn^{III}(PS2)_2]$ to stand in a closed test tube. After air was slowly introduced for several days, purple plates began to form from the solution.

UV-VIS: λ_{max}, nm(ε_m, $M^{-1}cm^{-1}$) = 275 (602000), 379 (105000), 534 (71600); 1.0 mM in CH_2Cl_2

Electrochemistry: $E_{1/2}$ (ΔE_P) = 191 mV (117 mV) 1.0 mM in DMF vs. Ag/AgCl, reduction

Synthesis of $[Bu_4N][Cr^{III}(PS2)_2]$:

$H_2[PS2]$ [0.500 g (1.53 mmol)] and lithium wire [0.0230 g (3.31 mmol)] were placed in a Schlenk flask and dissolved in 35 mL of methanol. Into another Schlenk flask was added $Cr^{II}_2(OAc)_4 \cdot 2H_2O$ [0.280 g (0.744 mmol)]. Using a cannula, the $Li_2[PS2]$ solution was quickly added to the awaiting $Cr^{II}_2(OAc)_4 \cdot 2H_2O$. Immediately, the solution turned a dark red-brown. The reaction was left to stir overnight. The next day, $(Bu_4N)Br$

[0.260 g (0.807 mmol)] was dissolved in 10 mL of methanol and added to the reaction mixture drop wise, using a cannula. After several minutes a dark red-brown microcrystalline precipitate was seen. After overnight standing, the mixture was filtered and the product was dried *in vacuo*. The reaction yielded 0.568 g (0.602 mmol, 78.2% yield) of product as dark red microcrystals.

Crystals were obtained by allowing a solution of $Li[Cr^{III}(PS2)_2]$ dissolved in methanol to be slowly layered onto an awaiting concentrated solution of Bu_4NBr also dissolved in methanol. Upon standing for several days red/brown crystals were formed.

UV-VIS: λ_{max}, nm(ε_m, $M^{-1}cm^{-1}$) = 288 (546000), 350 (143000); 1.0 mM in CH_2Cl_2

Electrochemistry: $E_{1/2}$ (ΔE_P) = 725 mV (77 mV) 1.0 mM in CH_2Cl_2 vs. Ag/AgCl, oxidation

Synthesis of $[Bu_4N][Cr^{III}(PS2')_2]$:

$H_2[PS2']$ [0.500 g (1.40 mmol)] and lithium metal [0.0200 g (2.88 mmol)] were placed in a Schlenk flask and dissolved in 35 mL of methanol. To a separate Schlenk flask, $Cr^{II}_2(OAc)_4 \cdot 2H_2O$ [0.260 g (0.691 mmol)] was added. The $Li_2[PS2']$ solution was transferred via cannula to the $Cr^{II}_2(OAc)_4 \cdot 2H_2O$ solid. Immediately the solution changed to a dark red color. The reaction mixture was stirred overnight. The following day, $(Bu_4N)Br$ [0.240 g (0.744 mmol)] was dissolved in 10 mL of methanol. This solution was added drop wise to the reaction mixture, via cannula. After several minutes a dark red-brown microcrystalline precipitate was seen. The flask was left to sit overnight. The

next day, the solid was filtered and dried *in vacuo* to yield 0.435g (0.442 mmol, 62.3% yield) of red-black microcrystalline product.

Crystals were grown by allowing a solution of $Li[Cr^{III}(PS2')_2]$ dissolved in methanol to be slowly layered onto an awaiting concentrated solution of Bu_4NBr also dissolved in methanol. Upon standing for several days red/brown crystals were formed.

UV-VIS: λ_{max}, nm(ε_m, $M^{-1}cm^{-1}$) = 289 (566000), 352 (150000); 1.0 mM in CH_2Cl_2

Electrochemistry: $E_{1/2}$ (ΔE_P) = 692 mV (70 mV) 1.0 mM in CH_2Cl_2 vs. Ag/AgCl, oxidation

Synthesis of $[Cr^{IV}(PS2)_2]$:

$[Bu_4N][Cr^{III}(PS2)_2]$ [0.250 g (0.310 mmol) of] was placed in a Schlenk flask and dissolved in 30 mL of acetonitrile. To a separate Schlenk flask, $(Fc)BF_4$ [0.084 g (0.310 mmol)] was dissolved in 15 mL of acetonitrile. This $(Fc)BF_4$ solution was cannulaed over quickly to the former solution and left to stir for two days. It was then observed that a dark green precipitate was formed. This mixture was filtered and the product was dried *in vacuo* to yield 0.048 g (0.069 mmol, 22% yield) of product.

UV-VIS: λ_{max}, nm(ε_m, $M^{-1}cm^{-1}$) = N/A

Electrochemistry: $E_{1/2}$ (ΔE_P) = 939 mV (83 mV) 1.0 mM in CH_2Cl_2 vs. Ag/AgCl, reduction

Irreversible reduction at 657 mV

Synthesis of $[Pr_4N][Mo^{III}(PS2)_2]$:

Lithium metal [0.030 g (4.32 mmol)] was dissolved in 35 mL of methanol in a Schlenk flask. $H_2[PS2]$ [0.500 g (0.153 mmol)] was then added to the solution. To a separate Schlenk flask, $Mo^{III}Cl_3(THF)_3$ [0.030 g (0.073 mmol)} was added. The $Li_2[PS2]$ solution was then cannulaed over quickly to the $Mo^{III}Cl_3(THF)_3$ solid. Immediately, the solution turned a dark green color. This mixture was refluxed for 3 hours. $(Pr_4N)Br$ [0.200 g (0.754 mmol)] was dissolved in 15 mL of methanol in a separate Schlenk flask and slowly cannulaed over to the reaction mixture, now at room temperature. Immediately, a green microcrystalline precipitate was seen coming out of the solution. The product was filtered and dried *in vacuo* to yield 0.565 g (0.609 mmol, 81.9% yield) of green product.

A crystal of $[Pr_4N][Mo^{III}(PS2)_2]$ was grown by allowing a solution of $Li[Mo^{III}(PS2)_2]$ in methanol to be slowly layered onto a solution of Pr_4NBr also in methanol. After standing for several days dark green crystals were formed.

UV-VIS: λ_{max}, nm(ε_m, $M^{-1}cm^{-1}$) = 379 (92100); 1.0 mM in CH_2Cl_2

Electrochemistry: $E_{1/2}$ (ΔE_P) = 4 mV (140 mV) 1.0 mM in CH_2Cl_2 vs. Ag/AgCl, oxidation

Synthesis of $[Mo^{IV}(PS2)_2]$:

$[Pr_4N][Mo^{III}(PS2)_2]$ **[**0.150 g (0.161 mmol)] was dissolved in 20 mL of acetonitrile in a Schlenk flask. $(Fc)BF_4$ **[**0.048 g (0.176 mmol)] was dissolved in 10 mL of acetonitrile in a separate Schlenk flask. After four hours, some green-brown

precipitate was seen forming in the solution. The reaction was left to stir overnight. The following day the precipitate was filtered and dried to yield 0.042 g (0.054 mmol, 33.5% yield) of $[Mo^{IV}(PS2)_2]$. The filtrate was dried *in vacuo* and 20 mL of methanol was added to the filtrate. After several hours of stirring, the precipitate was filtered and dried *in vacuo* to yield an additional 0.021 g (0.081 mmol, 50.3% yield) of product.

A crystal of $[Mo^{IV}(PS2)_2]$ was grown by allowing drying the acetonitrile from the filtrate of the reaction described above. Methanol was then added to the residue and allowed to stand for one week. After a week, small purple crystals were observed.

UV-VIS λ_{max}, nm(ε_m, $M^{-1}cm^{-1}$) = 330 (12900), 367 (90300), 406 (84300), 494 (90900); 1.0 mM in CH_2Cl_2

Electrochemistry: $E_{1/2}$ (ΔE_P) = 184 mV (157 mV) 1.0 mM in CH_2Cl_2 vs. Ag/AgCl, reduction

Results and Discussion

The following crystals structures were all found to have several properties in common. Most importantly all of the structures had two [PS2] ligands both coordinated as tridentate ligands to the metal center, forming a distorted octahedral geometry with formulation, $[M(PS2)_2]^n$ (n = 0, -1). The phosphorus atoms for each complex were *cis* to each other. The fact that the bond angle of the *trans* atoms are always significantly less than the ideal 180° is due to the fact that the native H_2[PS2] ligand has a low bite angle (ca. 79-85°)[10]. Concerning the electrochemical studies it must always be taken into account that the ligand itself could be oxidized or reduced. Specifically, the thiolate donors have a potential to be oxidized to a thiolate radical. However, this was ruled out for the complexes below as ligand oxidation/reductions are irreversible processes and occur at much higher potentials than observed below[11]. The UV-VIS spectra obtained from each sample showed the peaks that are associated with a metal-to-ligand charge transfer.

Within this work is the discovery that the [PS2] ligand stabilizes metal complexes in high formal oxidation states. For instance, such compounds as $[M^{III}(PS2)_2]^-$ and $[M^{IV}(PS2)_2]$ have been synthesized and/or electrochemically characterized. This is a significant result. Usually, metals in high oxidation states, such as Fe(III), react with thiolates (RS^-) to form disulfide (by an oxidation process) and Fe(II) (by a reduction process). This over all reaction is called an auto-redox reaction:

$$2\ Fe(III) + 2\ RS^- \rightarrow 2\ Fe(II) + RSSR \quad (2)$$

It is through that, in the complexes of [PS2], the chelate ring may add something to the stability of the M-SR interaction. Some notable examples of other metal-thiolate

complexes in high formal oxidation states include those stabilized by sterically encumbered ligands as discovered in the Millar group and the Koch group. Such examples include Fe(III)-RS complexes[22,23,24,25], Ru(IV)-SR complexes[26,27,28,29] and Co(III)-SR[30].

Vanadium Complexes:

Crystals of $[Et_4N][V^{III}(POS2)_2]$ were grown by allowing a vapor diffusion of CH_2Cl_2/hexanes to stand for one week at -20°C. Note that this complex was not synthetically isolated.

Both V(III) and V(IV) complexes were synthesized and characterized with single crystal X-ray diffraction. The bond lengths of the coordinating atoms to each metal centered differed as expected between the two structures. The V(III) complex had an average V – S bond distance of 2.3969 Å, while the V(IV) complex had an average distance of 2.3199 Å (a difference of 0.0770 Å). The average sulfur phosphorus bond lengths of the V(III) and V(IV) complex were 2.4408 Å and 2.4476 Å (a difference of 0.0068 Å), respectively. The sulfur metal bond distance of the V(III) complex is much longer than that of the V(IV) complex for simple reasons. The atomic radii of M(III) compounds are longer than that of M(IV) compounds. In addition, the V(IV) complex is electron poor compared to the V(III) complex and therefore forms a stronger bond to the negatively charged thiolate atom. By this latter logic, the metal phosphorus bond lengths between the two complexes are about the same. The phosphorus atom is neutral and therefore will not be more strongly or weakly bound to a metal based solely on the fact of how electron rich or poor it may be.

The bond angles between the two complexes do differ by slight amounts. The majority of the angles differ by at most five degrees. The differences in the bond angles can be explained by the same reasoning above. Because the thiolates are more closely bonded in the V(IV) complex, the bond angles will be altered as a result.

The $[Et_4N][V^{III}(PS2)_2]$ and $[Et_4N][V^{III}(POS2)_2]$ complexes have different bond lengths and angles as well. The former complex was found to have an average V – S bond length of 2.3969 Å. The latter complex was found to have an average bond length of 2.4278 Å. This bond length is in fact longer than that of the V(IV) complex, which had an average V – S bond length of 2.3199Å. The bond angles of the two complexes are mostly different for the reason that the ligands are different. These differences could be attributed to the fact that the [PS2] and [POS2] are very different ligands structurally, so it is not expected that their bond lengths and angles are comparable. Additionally, both structures have the same octahedral geometry. The oxygen atoms of the POS2 ligands are *cis* to each other just as the phosphorus atoms of the [PS2] ligands are *cis* to each other.

A similar octahedral V(IV) complex with two phosphorus and four sulfur donor atoms was found in the literature[11]. The ligand used in the literature is essentially two [PS2] ligands attached to each other with a disulfide bond, forming a hexadentate ligand. This bond was formed as a result of the free thiolate groups on the PS3 ligand reducing the V(V) to V (IV) with the formation of a disulfide The bond distances of the V(IV) compound reported here are similar to the compound reported in the literature[11]. The average V - S bond distance was found to be 2.3199Å whereas in the literature it is 2.324 Å. The average V - P bond length was found to be 2.4476 Å while in the literature it is

found to be 2.471 Å. These insignificant differences are due to the fact that the ligands are nearly identical.

The bond angles of each complex were not expected to be the same. This is due to the fact that the disulfide bond in the one ligand creates a strain in the complex. Many of the bond angles support this conclusion (only a few of those will be discussed here). The S3 – V1 – P1 bond angle found in the literature was 156.88° whereas here it was found to be 165.13°. Here the disulfide linkage creates a strain that pushes the S3 and P1 atoms closer together creating the smaller bond angle. The P1 – V1 – P2 bond angle in the literature is reported as 106.74° while here it was found to be 98.419°. In this case the disulfide linkage of the complex in the literature creates a strain that pushes the two phosphorous atoms closer together.

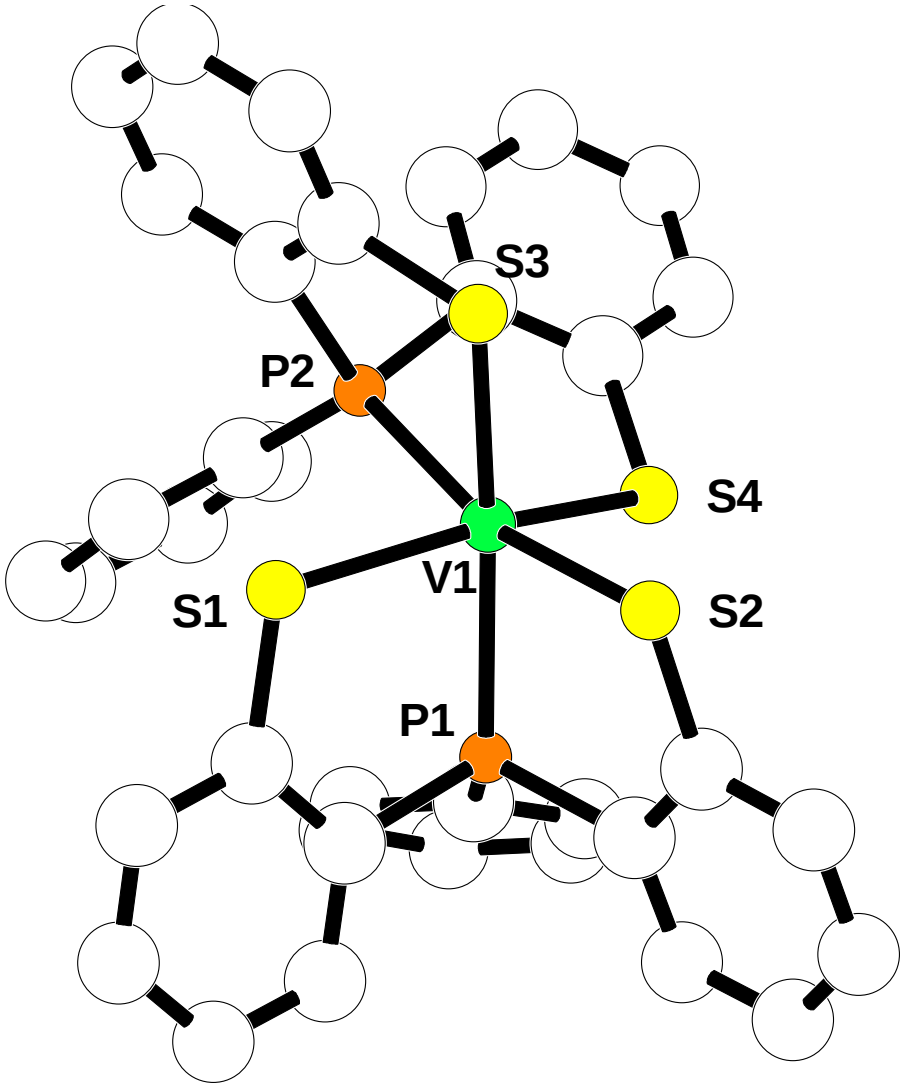

Figure 3: CHARON diagram of $[Et_4N][V^{III}(PS2)_2]$ (with the cation and hydrogens omitted for clarity).

Table 1a: Selected bond lengths for $[Et_4N][V^{III}(PS2)_2]$.

Atoms	Length (Å)
V1 – S1	2.3951(4)
V1 – S2	2.3904(4)
V1 – S3	2.4088(4)
V1 – S4	2.3934(4)
V1 – P1	2.4472(4)
V1 – P2	2.4343(4)

Table 1b: Selected bond angles for $[Et_4N][V^{III}(PS2)_2]$.

Atoms	Bond Angles (°)
S2 - V1 - S4	92.943(15)
S2 - V1 - S1	104.615(15)
S4 - V1 - S1	155.604(17)
S2 - V1 - S3	91.201(14)
S4 - V1 - S3	105.900(15)
S1 - V1 - S3	90.766(15)
S2 - V1 - P2	165.975(16)
S4 - V1 - P2	80.227(14)
S1 - V1 - P2	85.764(14)
S3 - V1 - P2	79.073(14)
S2 - V1 - P1	81.731(14)
S4 - V1 - P1	84.841(14)
S1 - V1 - P1	81.159(14)
S3 - V1 - P1	167.510(16)
P2 - V1 - P1	109.581(15)

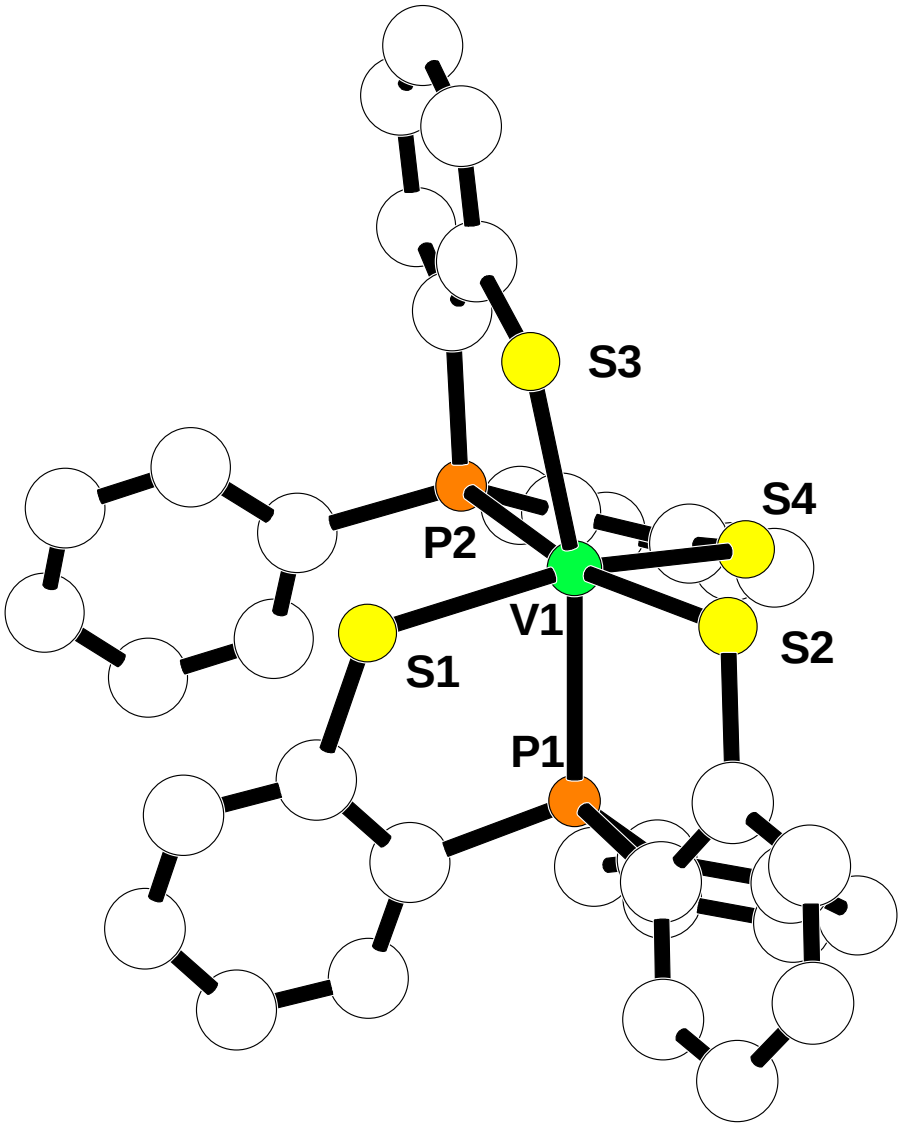

Figure 4: CHARON diagram of [$V^{IV}(PS2)_2$] (with hydrogens omitted for clarity).

Table 2a: Selected bond lengths for $[V^{IV}(PS2)_2]$.

Atoms	Length (Å)
V1 - S1	2.3238(6)
V1 - S2	2.3237(6)
V1 - S3	2.3223(5)
V1 - S4	2.3096(6)
V1 - P1	2.4365(5)
V1 - P2	2.4587(6)

Table 2b: Selected bond angles for $[V^{IV}(PS2)_2]$.

Atoms	Bond Angles (°)
S4 - V1 - S3	108.79(2)
S4 - V1 - S2	88.39(2)
S3 - V1 - S2	94.321(19)
S4 - V1 - S1	157.00(2)
S3 - V1 - S1	87.25(2)
S2 - V1 - S1	107.21(2)
S4 - V1 - P1	86.069(19)
S3 - V1 - P1	165.13(2)
S2 - V1 - P1	85.362(18)
S1 - V1 - P1	78.682(19)
S4 - V1 - P2	78.90(2)
S3 - V1 - P2	85.349(18)
S2 - V1 - P2	166.41(2)
S1 - V1 - P2	86.35(2)
P1 - V1 - P2	98.419(18)

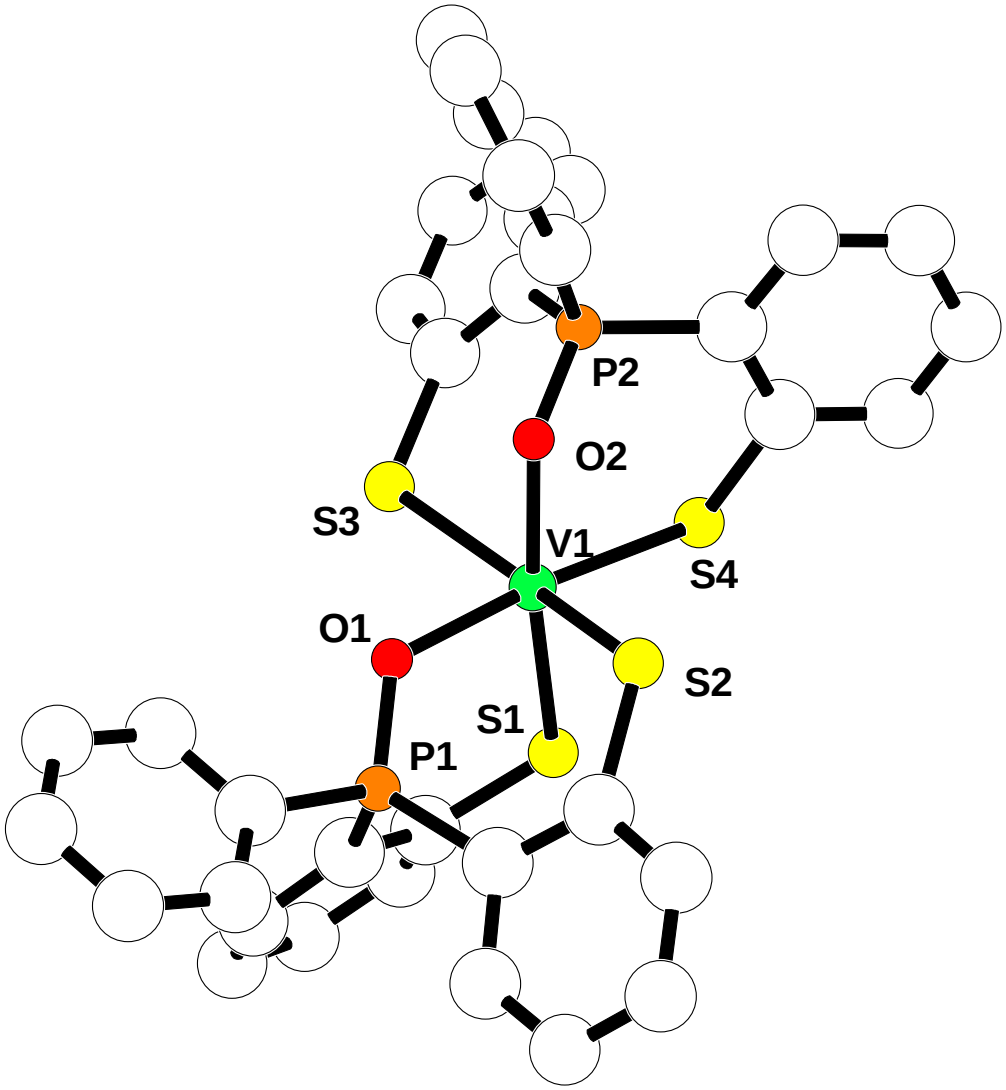

Figure 5: CHARON diagram of $[Et_4N][V^{III}(POS2)_2]$ (with the cation and hydrogens omitted for clarity).

Table 3a: Selected bond lengths for $[Et_4N][V^{III}(POS2)_2]$

Atoms	Length (Å)
V1 – S1	2.4275(15)
V1 – S2	2.4153(14)
V1 – S3	2.4340(14)
V1 – S4	2.4344(14)
V1 – O1	2.039(3)
V1 – O2	2.046(3)
O1 – P1	1.511(3)
O2 – P2	1.508(3)

Table 3b: Selected bond angles for $[Et_4N][V^{III}(POS2)_2]$

Atoms	Bond Angles (°)
O1 - V1 - O2	96.51(12)
O1 - V1 - S2	85.31(9)
O2 - V1 - S2	82.83(9)
O1 - V1 - S1	90.33(9)
O2 - V1 - S1	173.11(10)
S2 - V1 - S1	96.91(5)
O1 - V1 - S3	82.68(9)
O2 - V1 - S3	83.66(9)
S2 - V1 - S3	160.76(6)
S1 - V1 - S3	98.14(5)
O1 - V1 - S4	172.76(10)
O2 - V1 - S4	90.72(9)
S2 - V1 - S4	95.99(5)
S1 - V1 - S4	82.45(5)
S3 - V1 - S4	97.81(5)

The electrochemistry of the V(III) complex yielded interesting results. As the sample was left to stand, the spectrum changed significantly. The initial reversible oxidation peak to V(IV) became less intense, while another reversible oxidation peak was observed gaining intensity. This observation was later explained with the isolation of the $[Et_4N][V^{III}(POS2)_2]$ complex. Initially a crystal of a $[Et_4N][V^{III}(PS2)_2]$ was attempted to be grown in a CH_2Cl_2/hexanes vapor diffusion at -20°C. A crystal was grown, and the structure was solved to be the $[Et_4N][V^{III}(POS2)_2]$ complex. The following explains how this structure was believed to be generated.

It was determined that initially in the CV cell the $[Et_4N][V^{III}(PS2)_2]$ was being oxidized and then reduced to $V^{IV}(PS2)_2$. After standing for some time, a second reversible oxidation peak was seen. As time progresses the initially more intense peak becomes less intense as the second, initially absent peak, becomes more intense. This indicates that the initial species, $[V^{III}(PS2)_2]^-$, is slowly converting to $[V^{III}(POS2)_2]^-$ (as the intensity of the peaks is directly proportional to the concentration was what is being oxidized or reduced). After about the passage of thirty minutes only $[V^{III}(POS2)_2]^-$ remains in solution. With the passage of time a color change of the solution was also noted. Initially the solution is an intense dark red color. After thirty minutes the solution becomes a slightly less dark red and markedly less intense.

Interestingly, an isolated $[W^{IV}(PS2)_2]$ complex was shown to undergo a similar transformation. Upon the addition of oxygen to this complex, a [WO(PS2)(POS2)] complex was isolated and characterized using single crystal X-ray diffraction[12]. That is why it is believed that oxygen is responsible for the transformation above as well. However, only one phosphorus atom was oxidized in the complex, while here both phosphorus centers were oxidized. Nonetheless it is still most likely the case that oxygen is responsible for this transformation.

There is a large difference between the $E_{1/2}$ of the V(III) and V(IV) complexes. It was expected that these values would be around the same due to the fact that each complex has nearly identical connectivity of the ligands. In other words, it was expected that the same voltage would be required to oxidize the V(III) complex as would be to reduce the V(IV) complex. However the $E_{1/2}$ for the V(IV) complex was 222 mV while for the V(III) complex it was 385 mV. This difference can be explained by the following

reasoning. It is possible when reduced the V(III) complex forms a complex different from the isolated V(IV) complex. For example, the V(IV) complex created electrochemically could have the phosphorus *trans* to one another instead of *cis*.

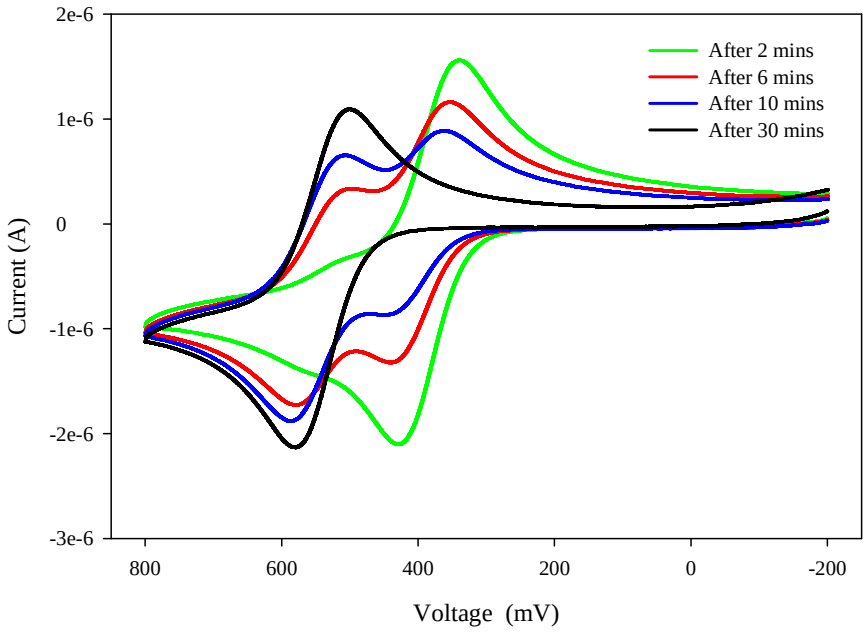

Figure 6: CV spectra of $[Et_4N][V^{III}(PS2)_2]$.

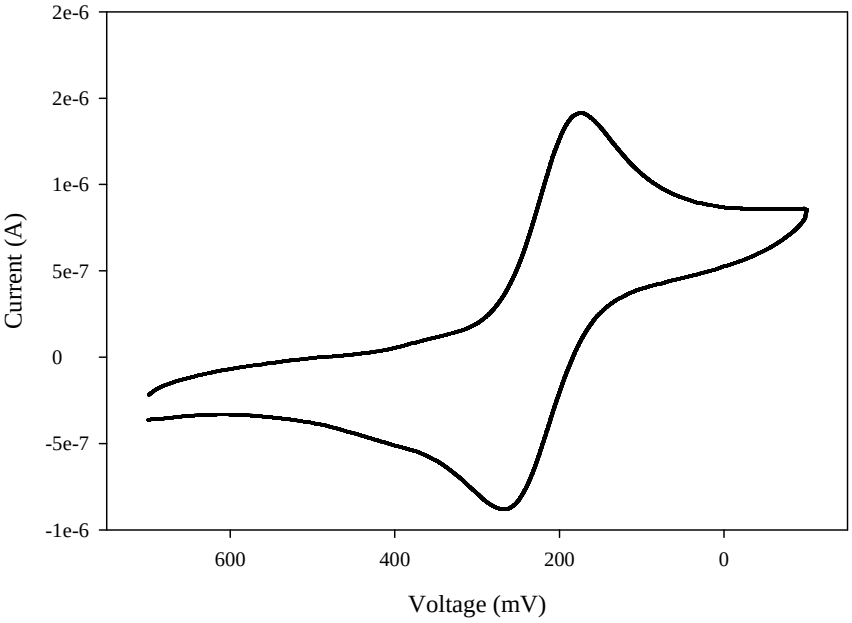

Figure 7: CV spectrum of $[V^{IV}(PS2)_2]$.

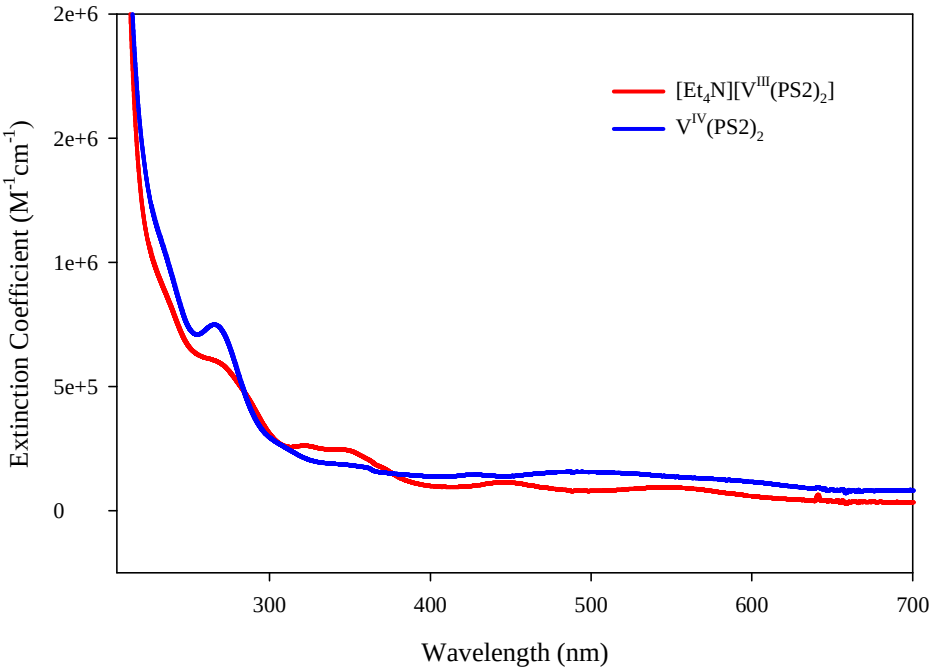

Figure 8: UV-VIS spectra of selected vanadium complexes (0.1 mm path length).

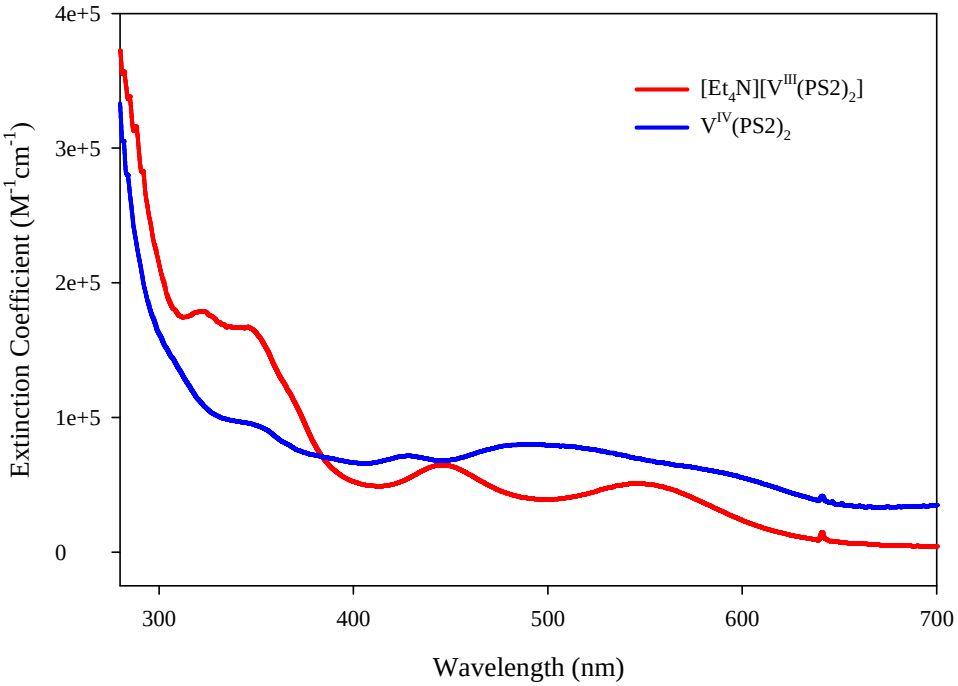

Figure 9: UV-VIS spectra of selected vanadium complexes (1.0 mm path length).

Manganese Complexes:

Two manganese complexes were synthesized, both with two [PS2'] ligands coordinated to the metal center. One was a Mn(III) complex, the other a Mn(IV) complex. It was predicted that the bond lengths of Mn to each thiolate sulfur atom would be shorter for the Mn(IV) complex than for the Mn(III) complex for the same reason as stated above. However, this was not entirely observed. The Mn – S bond lengths for each complex were almost identical except for the Mn – S4 bond length. This bond length was the only one to be shorter in the Mn(IV) complex than in the Mn(III) complex. It was also predicted that the Mn – P bond lengths would perhaps be unchanged between the two structures, as with the V complexes (for the same reason mentioned above). However, this too was not observed. The average Mn – P bond lengths for the Mn(III) complex were 2.2870 Å, while for the Mn(IV) complex the average length was 2.359 Å. This fact can be explained by the weakening of the *trans* effect due to the fact that Mn(IV) has one less electron than Mn(III). The fact that the Mn(III) complex would be expected to show a Jahn-Teller distortion, due to the presence of an electron in the e_g orbital also explains this observation. The bond angles of the two complexes vary accordingly. The angles for the most part are the same or close in value, within five degrees. Any difference in bond angles could be attributed to the fact that the metal center has a different number of electrons.

The bond angles and lengths of both the Mn(III) and Mn(IV) complexes are comparable to a previously synthesized $[Pr_4N][Mn^{III}(PS2)]$ and $Mn^{IV}(PS2)_2$ complexes[31]. The average Mn - S bond length for the Mn(III) complex synthesized here was 2.310 Å, while Beatty found it to be 2.301 Å. The average Mn – P bond length was found to be

2.287 Å, whereas Beatty observed a length of 2.290 Å. The Mn(IV) complex synthesized here was found to have an average Mn – S bond length of 2.304 Å. Beatty obtained an average bond length of 2.300 Å. The average Mn – P bond length in this work was found to be 2.359 Å. In Beatty's work the average length was 2.353 Å. An identical $Mn^{IV}(PS2)_2$ was also synthesized in the literature[10]. The average Mn – S and Mn – P bond lengths for this structure were found to be 2.3135 Å and 2.3584 Å respectively. These lengths are very similar to the ones observed in this work as well as Beatty's work.

The bond angles again here are unremarkable. Between the two Mn(III) complexes (the one synthesized here and the one synthesized by Beatty) there is not much variation in the bond angles. The three Mn(IV) complexes also show very similar bond angles around the metal center.

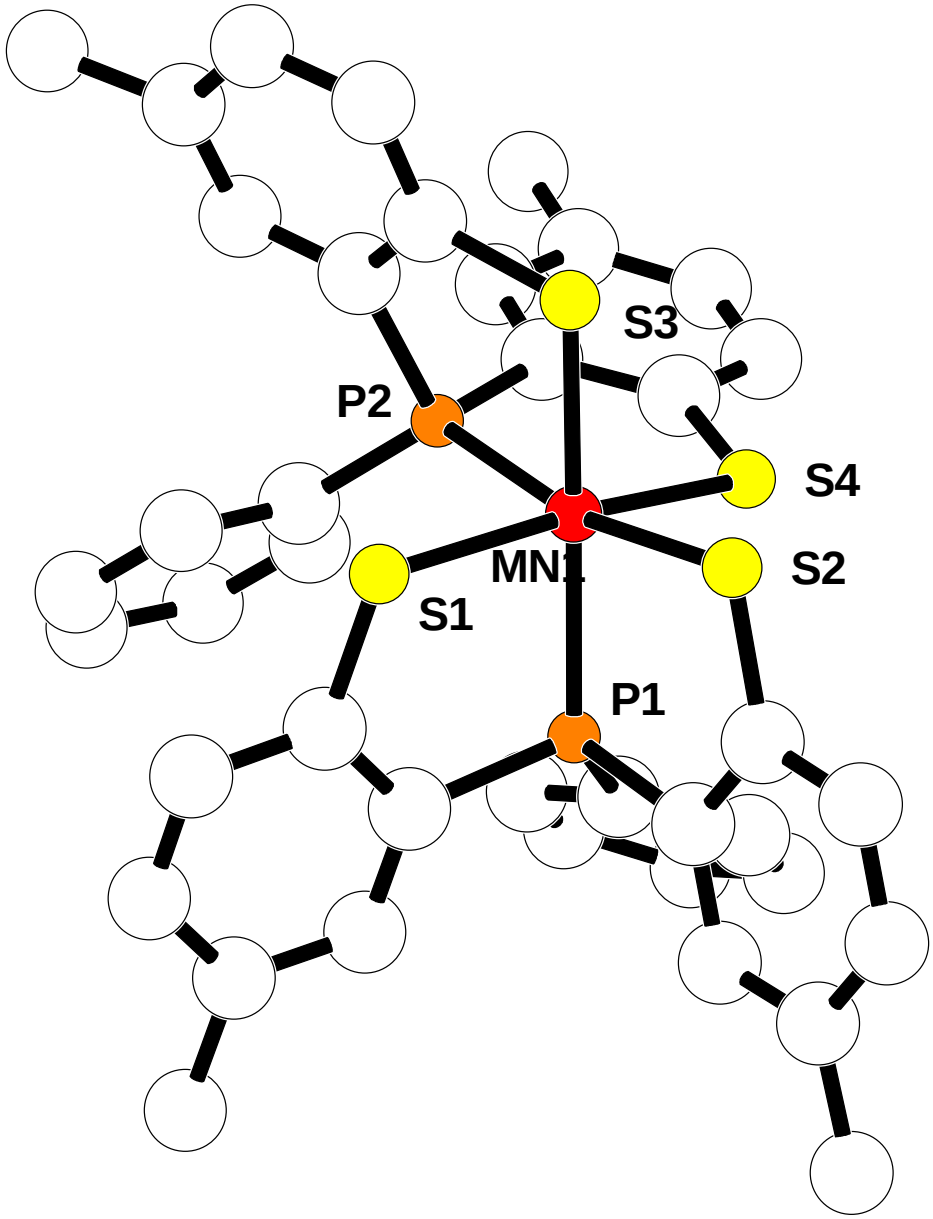

Figure 10: CHARON diagram of $[Et_4N][Mn^{III}(PS2')_2]$ (with the cation and hydrogens omitted for clarity).

Table 4a: Selected bond lengths for $[Et_4N][Mn^{III}(PS2')_2]$.

Atoms	Length (Å)
Mn1 - S1	2.3040(8)
Mn1 - S2	2.3106(8)
Mn1 - S3	2.2963(8)
Mn1 - S4	2.3298(8)
Mn1 - P1	2.2880(7)
Mn1 - P2	2.2860(8)

Table 4b: Selected bond angles for $[Et_4N][Mn^{III}(PS2')_2]$.

Atoms	Bond Angles (°)
P2 - Mn1 - P1	103.21(3)
P2 - Mn1 - S3	86.86(3)
P1 - Mn1 - S3	168.78(3)
P2 - Mn1 - S1	89.28(3)
P1 - Mn1 - S1	86.58(3)
S3 - Mn1 - S1	88.63(3)
P2 - Mn1 - S2	170.41(3)
P1 - Mn1 - S2	83.98(3)
S3 - Mn1 - S2	86.59(3)
S1 - Mn1 - S2	97.55(3)
P2 - Mn1 - S4	83.16(3)
P1 - Mn1 - S4	87.95(3)
S3 - Mn1 - S4	98.29(3)
S1 - Mn1 - S4	169.42(3)
S2 - Mn1 - S4	90.87(3)

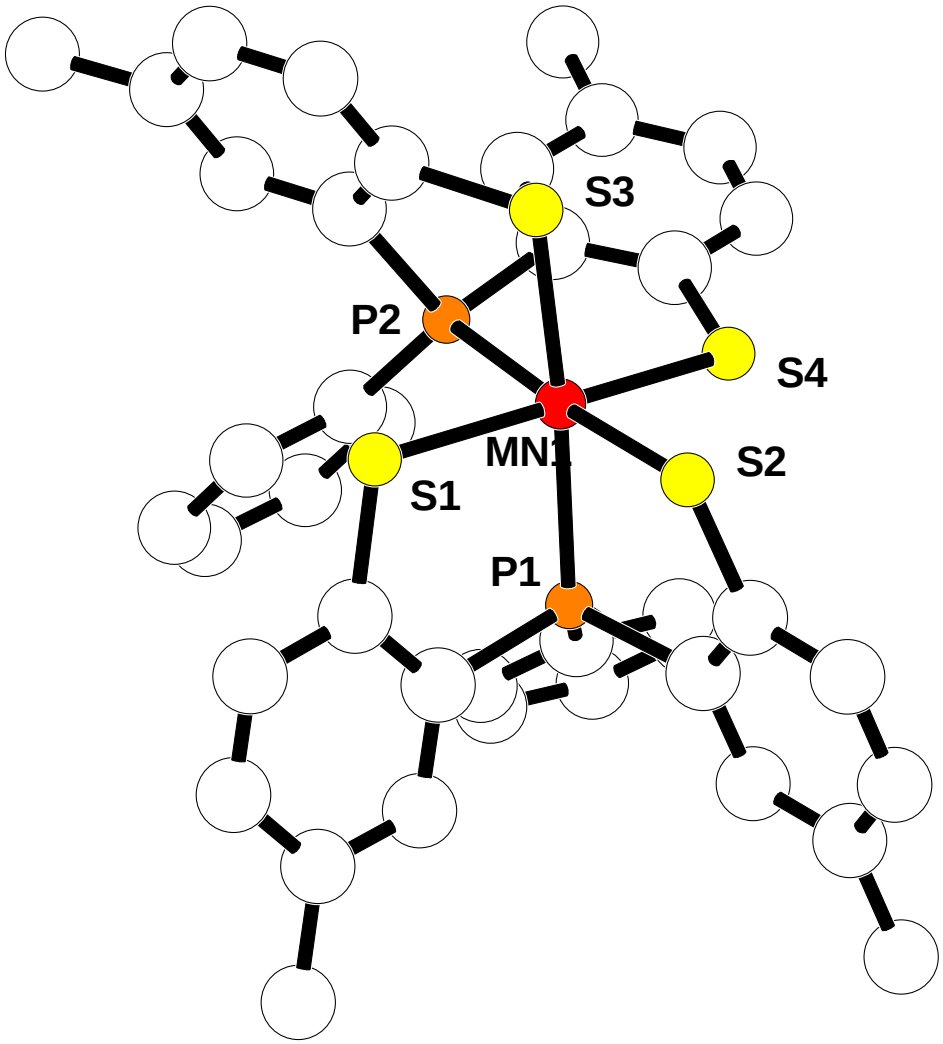

Figure 11: CHARON diagram of [$Mn^{IV}(PS2')_2$] (with the hydrogens omitted for clarity).

Table 5a: Selected bond lengths for $[Mn^{IV}(PS2')_2]$.

Atoms	Length (Å)
Mn1 - S1	2.303(2)
Mn1 - S2	2.315(2)
Mn1 - S3	2.302(2)
Mn1 - S4	2.297(2)
Mn1 - P1	2.362(2)
Mn1 - P2	2.356(2)

Table 5b: Selected bond angles for $[Mn^{IV}(PS2')_2]$.

Atoms	Bond Angles (°)
S4 - Mn1 - S3	94.42(9)
S4 - Mn1 - S1	170.44(9)
S3 - Mn1 - S1	89.55(8)
S4 - Mn1 - S2	89.32(9)
S3 - Mn1 - S2	97.05(9)
S1 - Mn1 - S2	98.83(9)
S4 - Mn1 - P2	86.49(7)
S3 - Mn1 - P2	81.94(8)
S1 - Mn1 - P2	85.47(7)
S2 - Mn1 - P2	175.59(9)
S4 - Mn1 - P1	90.44(8)
S3 - Mn1 - P1	175.12(9)
S1 - Mn1 - P1	85.57(8)
S2 - Mn1 - P1	83.48(8)
P2 - Mn1 - P1	97.90(7)

The electrochemistry of the Mn(III) and Mn(IV) complexes synthesized here led to an interesting conclusion. It was expected that each complex would have a similar $E_{1/2}$. This however was not the case and is problematic. The Mn(III) complex and the Mn(IV) complex had an $E_{1/2}$ of 311 mV and 191 mV, respectively. This observation could be explained using the same logic above. That is when the Mn(III) complex is oxidized electrochemically it forms a *trans, bis* [PS2] complex as opposed to when it is oxidized synthetically it forms a *cis, bis* [PS2] complex. The Mn(IV) could undergo a similar transformation when reduced. This is most likely the reason that the potentials

are not equal. Regardless, one complex must be oxidized or reduced into the *trans* isomer of the complex while the other must remain *cis*. If both were converted to a *trans* isomer than the $E_{1/2}$ potentials would also be the same. It is impossible to definitively determine if this is occurring as no *trans* isomer was isolated of either complex.

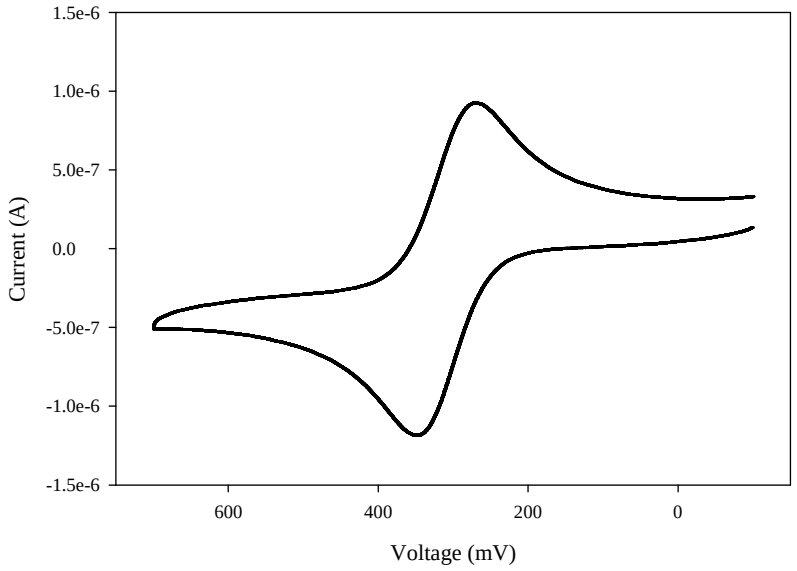

Figure 12: CV spectrum of $[Et_4N][Mn^{III}(PS2')_2]$.

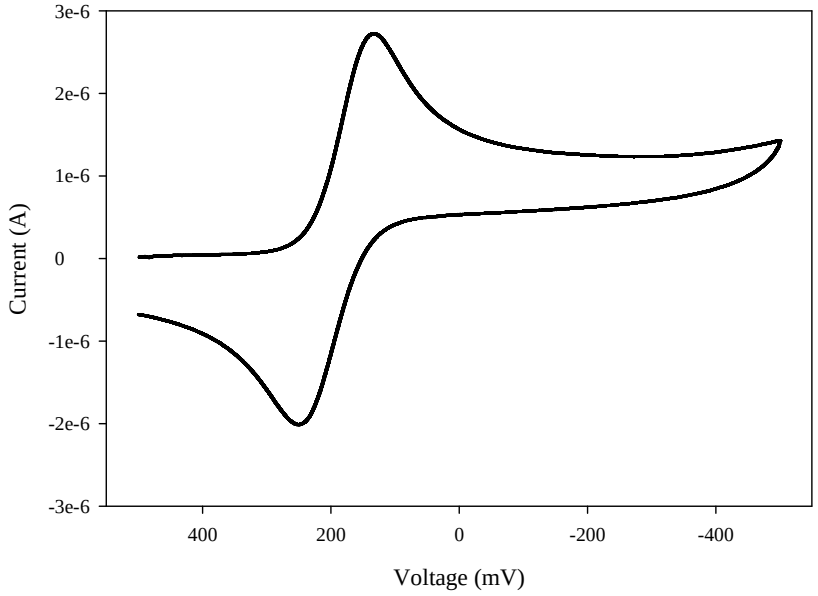

Figure 13: CV spectrum of $[Mn^{IV}(PS2')_2]$.

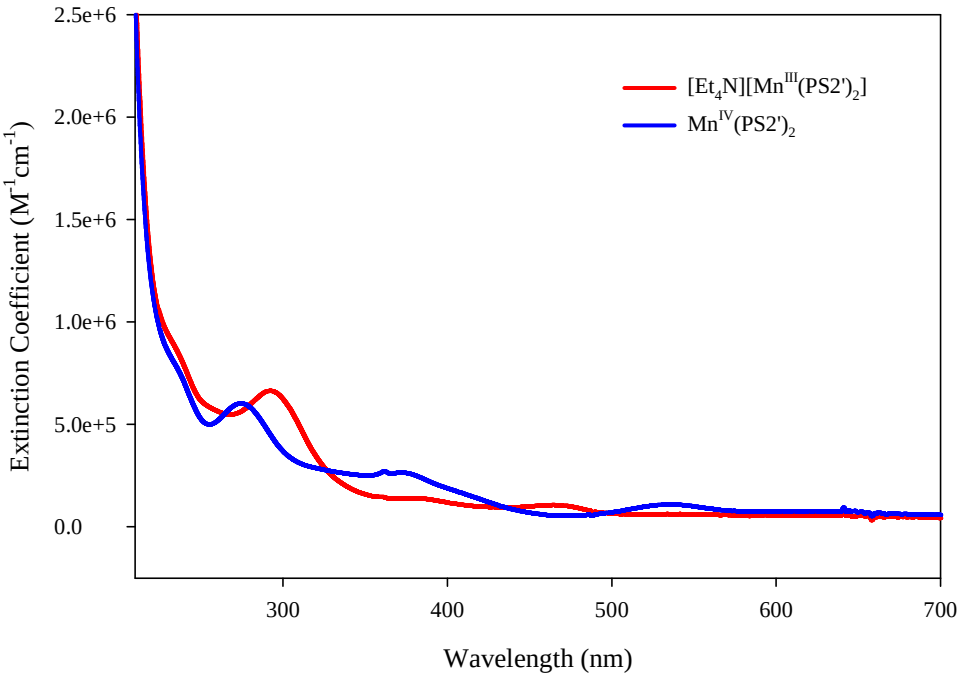

Figure 14: UV-VIS spectra of the manganese complexes (0.1 mm path length)

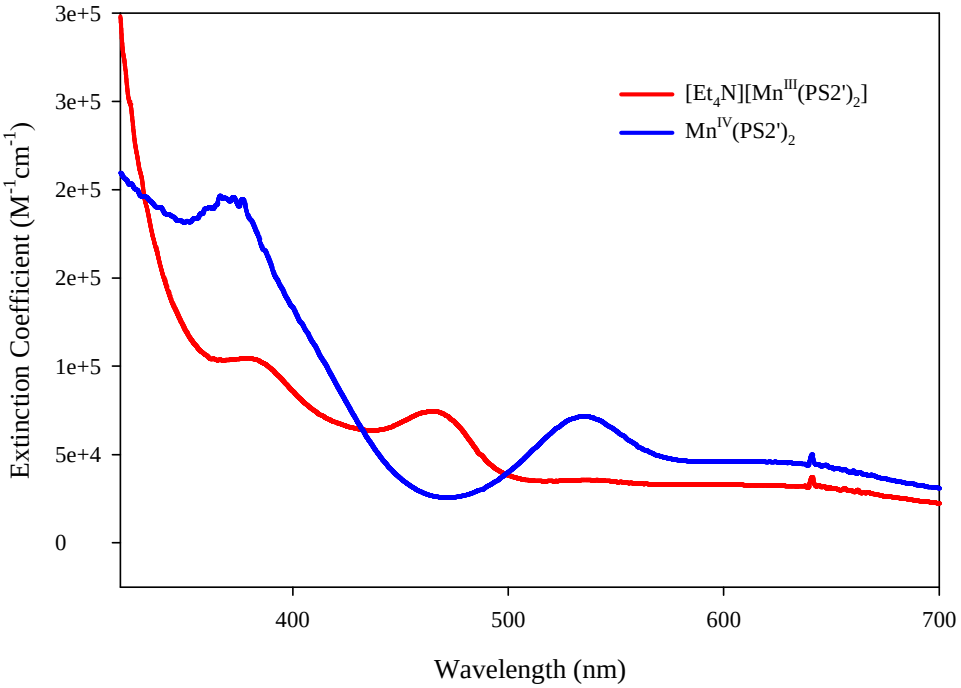

Figure 15: UV-VIS spectra of the manganese complexes (1.0 mm path length)

Chromium Complexes:

Two chromium complexes were synthesized, $[Bu_4N][Cr^{III}(PS2)_2]$ and $[Bu_4N][Cr^{III}(PS2')_2]$. Structurally the only difference between these complexes is the fact that the later complex has a methyl group *para* to the binding thiolate atom. As a result the differences in bond lengths do not differ greatly between the two complexes. The average Cr – S bond length for the $[Bu_4N][Cr^{III}(PS2)_2]$ complex was 2.3838 Å while for the $[Bu_4N][Cr^{III}(PS2')_2]$ the average bond length was 2.3750 Å. The average Cr – P bond length for the $[Bu_4N][Cr^{III}(PS2)_2]$ and $[Bu_4N][Cr^{III}(PS2')_2]$ complexes were 2.4068 Å and 2.3871 Å, respectively. The bond lengths around the metal center are slightly shorter for the $[Bu_4N][Cr^{III}(PS2')_2]$ complex than for the $[Bu_4N][Cr^{III}(PS2)_2]$ complex. This observation is due to the presence of an extra methyl group on the [PS2'] ligand. The methyl group acts as an electron donating group, causing the binding atoms (sulfur and phosphorous) to be more electron rich and thus bind more strongly to the metal. However, this difference in bond lengths is small as seen above.

The bond angles are not appreciably different between the two complexes. Most angles vary by about one or two degrees. This is so because sterically, the ligands [PS2] and [PS2'] are nearly identical. The fact that [PS2'] has a methyl group *para* to the thiolate functional group has little effect on the cone angle of the ligand. Had the methyl group been *ortho* to the thiolate functional group then the cone angle would be noticeably different and then a difference in the bond angles of each ligand to the metal could be seen. A *para* methyl group adds no steric difference to the ligand only an electronic difference. The differences between the bond angles can be explained by the different

unit cell that each complex formed as a single crystal. Because each complex is packed together differently, each one would have different bond angles.

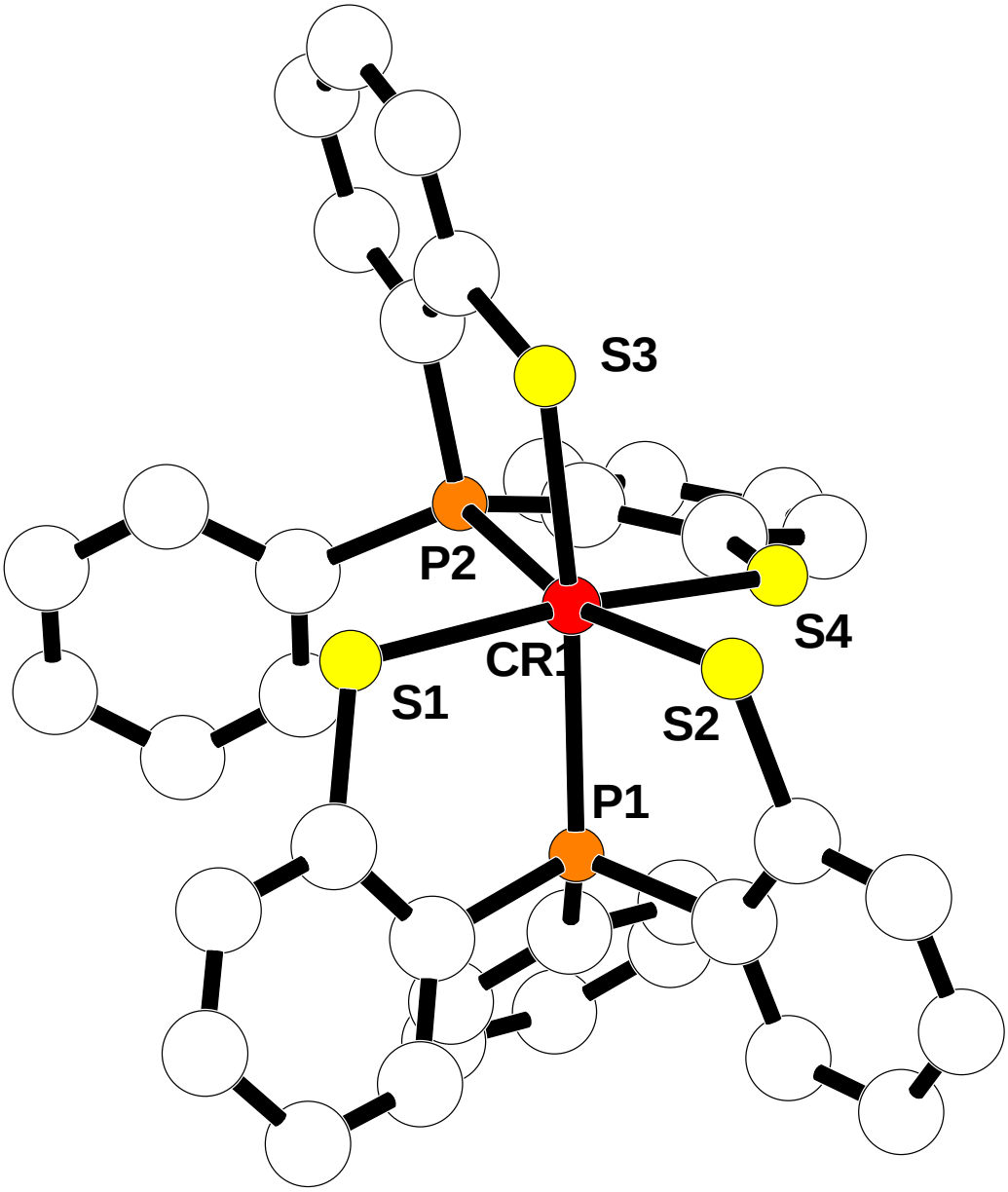

Figure 16: CHARON diagram of $[Bu_4N][Cr^{III}(PS2)_2]$ (with the cation and hydrogens omitted for clarity).

Table 6a: Selected bond lengths for $[Bu_4N][Cr^{III}(PS2)_2]$.

Atoms	Length (Å)
Cr1 – S1	2.3891(12)
Cr1 – S2	2.3831(11)
Cr1 – S3	2.3694(11)
Cr1 – S4	2.3897(11)
Cr1 – P1	2.3907(11)
Cr1 – P2	2.4229(12)

Table 6b: Selected bond angles for $[Bu_4N][Cr^{III}(PS2)_2]$.

Atoms	Bond Angles (°)
S3 - Cr1 - S2	90.17(4)
S3 - Cr1 - S1	86.11(4)
S2 - Cr1 - S1	100.03(4)
S3 - Cr1 - S4	101.85(4)
S2 - Cr1 - S4	85.81(4)
S1 - Cr1 - S4	170.19(4)
S3 - Cr1 - P1	165.19(5)
S2 - Cr1 - P1	82.14(4)
S1 - Cr1 - P1	82.82(4)
S4 - Cr1 - P1	90.25(4)
S3 - Cr1 - P2	85.02(4)
S2 - Cr1 - P2	165.20(5)
S1 - Cr1 - P2	93.62(4)
S4 - Cr1 - P2	81.50(4)
P1 - Cr1 - P2	105.41(4)

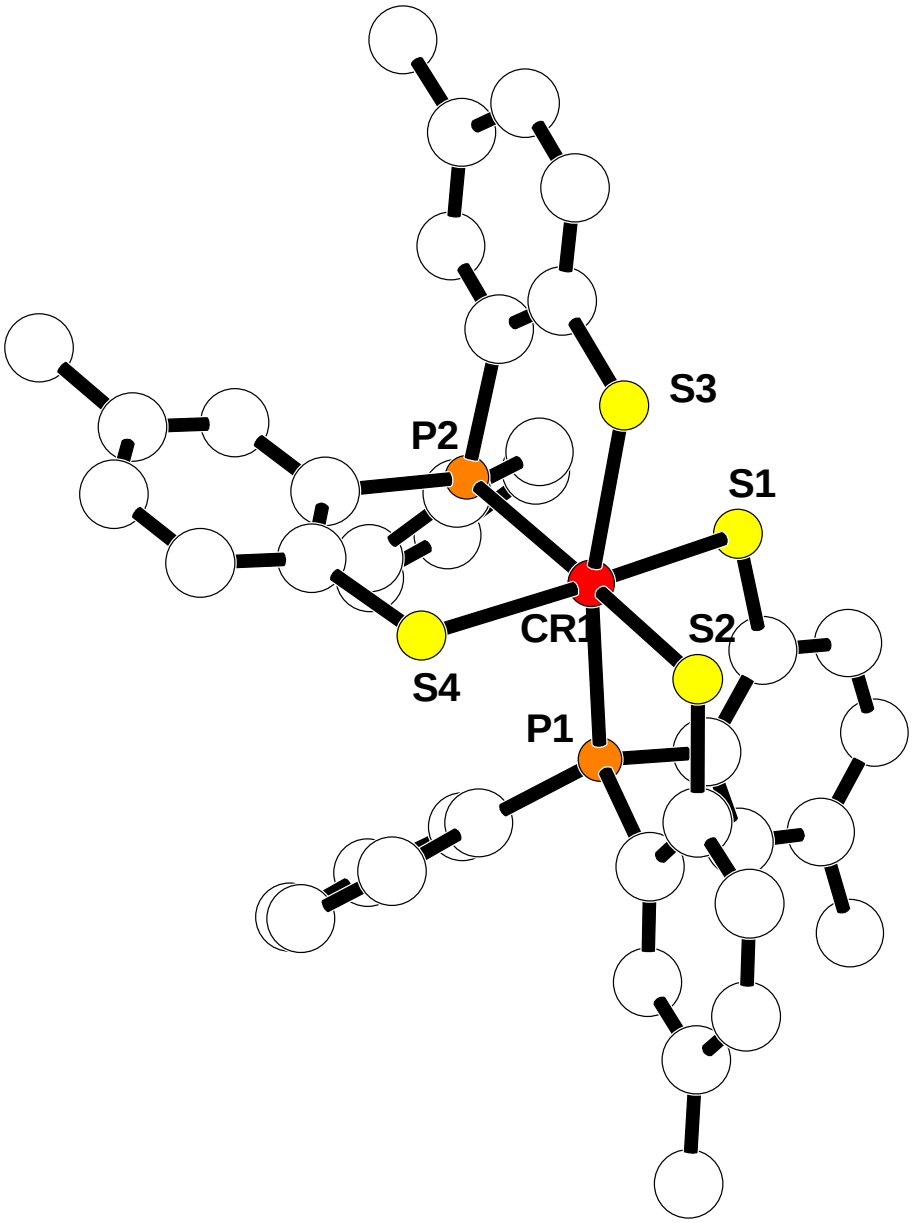

Figure 17: CHARON diagram of $[Bu_4N][Cr^{III}(PS2')_2]$ (with the cation and hydrogens omitted for clarity).

Table 7a: Selected bond lengths for $[Bu_4N][Cr^{III}(PS2')_2]$.

Atoms	Length (Å)
Cr1 - S1	2.3709(9)
Cr1 - S2	2.3601(9)
Cr1 - S3	2.3811(11)
Cr1 - S4	2.3880(10)
Cr1 - P1	2.3933(11)
Cr1 - P2	2.3808(10)

Table 7b: Selected bond angles for $[Bu_4N][Cr^{III}(PS2')_2]$.

Atoms	Bond Angles (°)
S2 - Cr1 - S1	99.89(3)
S2 - Cr1 - P2	170.72(4)
S1 - Cr1 - P2	87.71(3)
S2 - Cr1 - S3	91.18(3)
S1 - Cr1 - S3	86.93(3)
P2 - Cr1 - S3	83.87(4)
S2 - Cr1 - S4	89.24(3)
S1 - Cr1 - S4	169.28(3)
P2 - Cr1 - S4	83.77(3)
S3 - Cr1 - S4	98.57(4)
S2 - Cr1 - P1	83.65(3)
S1 - Cr1 - P1	83.67(3)
P2 - Cr1 - P1	102.60(3)
S3 - Cr1 - P1	168.32(4)
S4 - Cr1 - P1	91.84(4)

Electrochemically, both complexes are very similar. Both show a reversible one electron oxidation to a Cr(IV) species. The $[Bu_4N][Cr^{III}(PS2)_2]$ complex had its oxidation at 724 mV while the $[Bu_4N][Cr^{III}(PS2')_2]$ species had its oxidation at 692 mV. This suggests that it would take less energy for the complex with the extra methyl group to be oxidized than the complex without the methyl group. This is so because the methyl group is an electron donor. This extra electron donation serves to stabilize the more electron deficient Cr(IV) complex. Or said another way, the electron donating properties of the methyl group stabilizes the higher oxidation state. Thus it is easier to oxidize the $[Bu_4N][Cr^{III}(PS2')_2]$ complex and $[Cr^{IV}(PS2')_2]$ would be more stable than $[Cr^{IV}(PS2)_2]$.

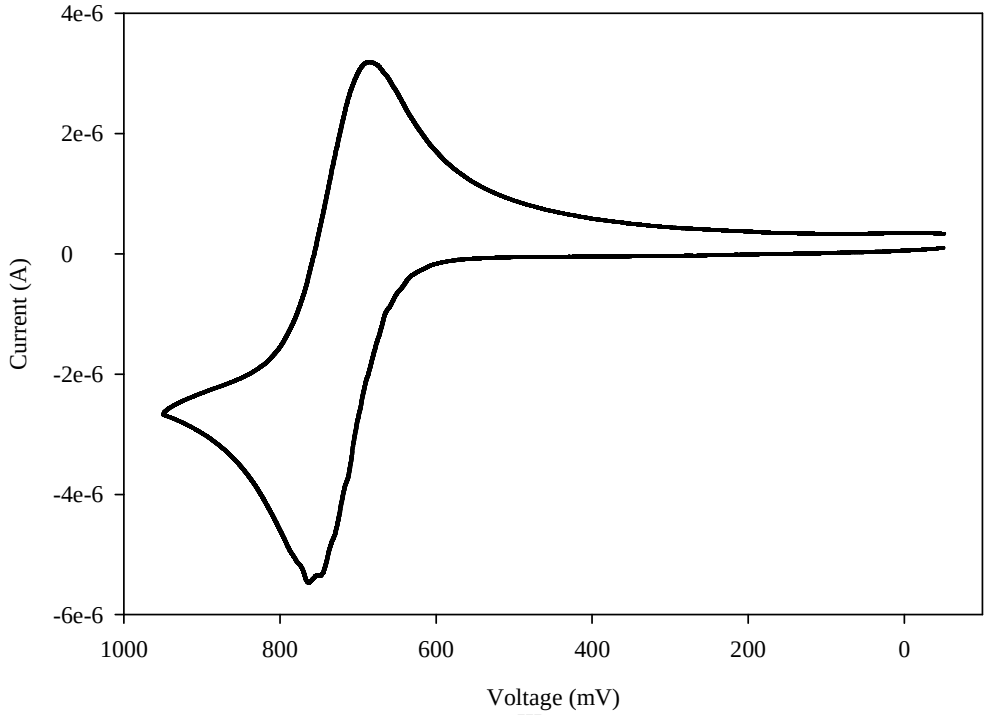

Figure 18: CV spectrum of $[Bu_4N][Cr^{III}(PS2)_2]$.

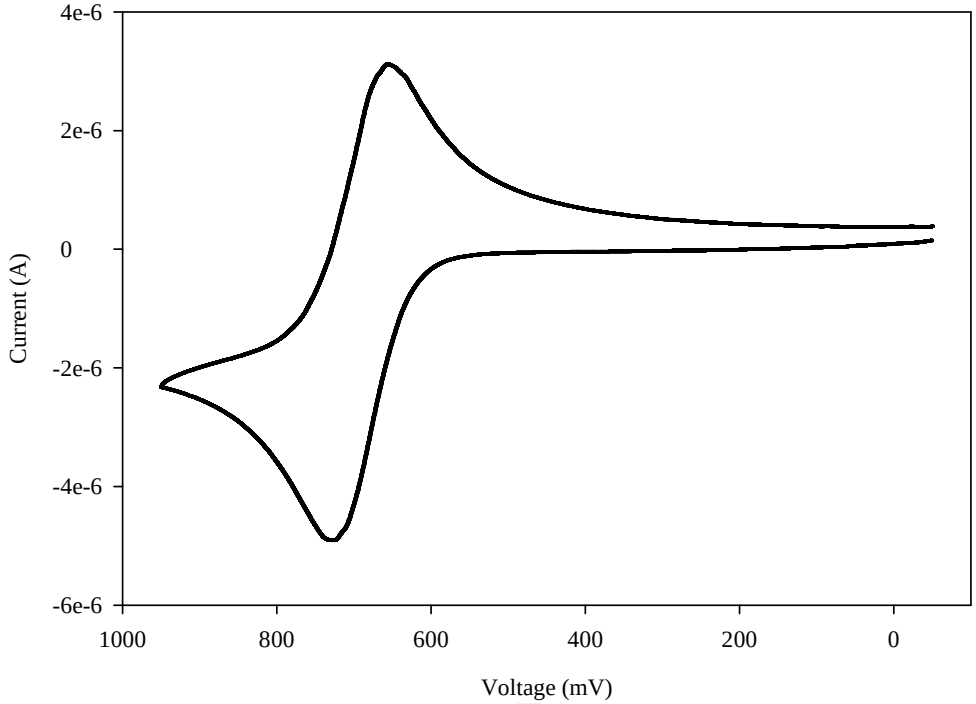

Figure 19: CV spectrum of $[Bu_4N][Cr^{III}(PS2')_2]$.

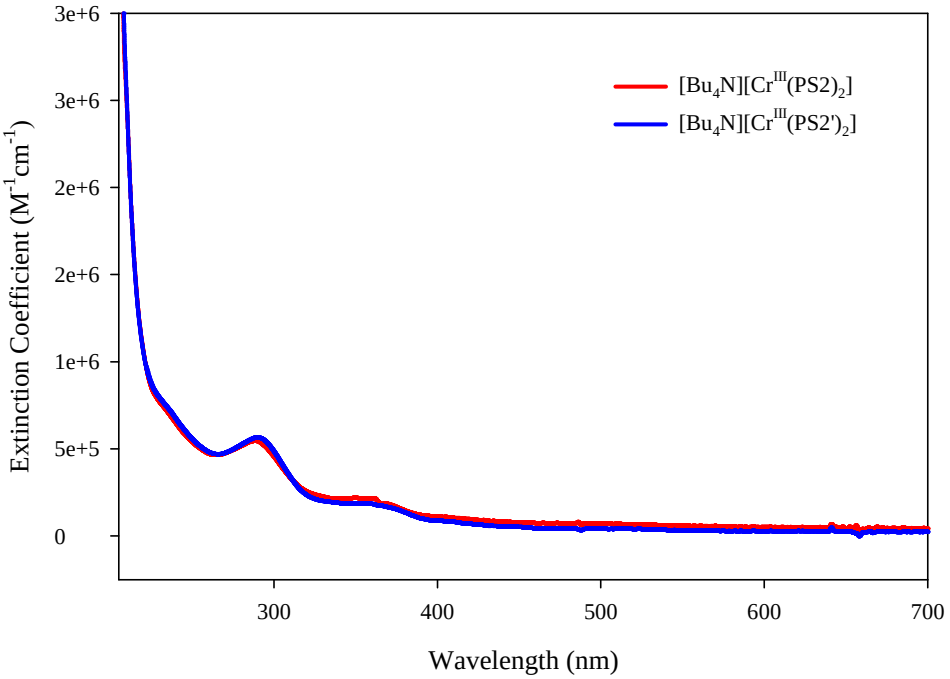

Figure 20: UV-VIS spectra of the chromium(III) complexes (0.1 mm path length).

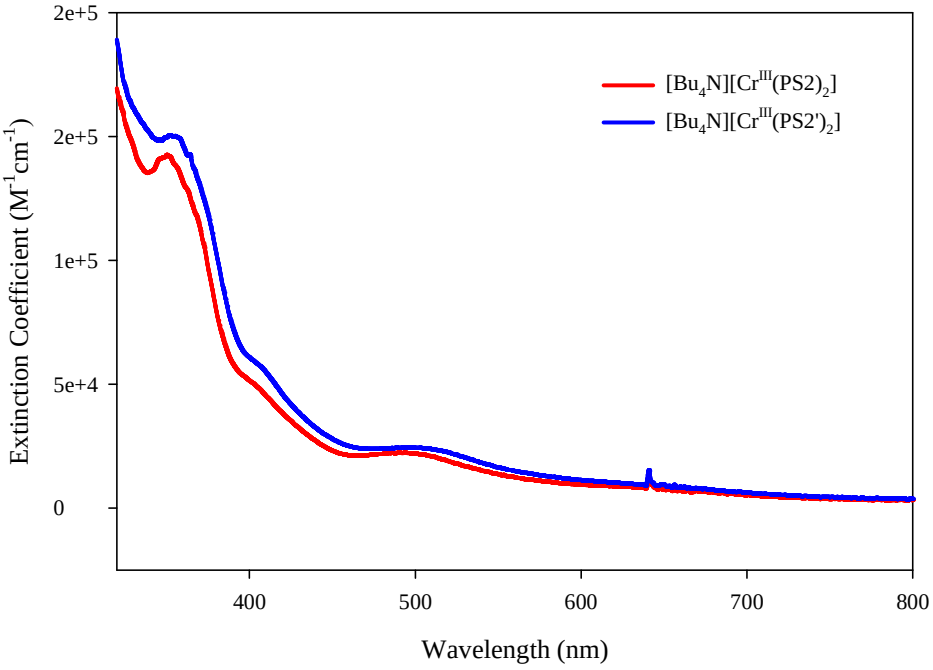

Figure 21: UV-VIS spectra of the chromium(III) complexes (1.0 mm path length).

A potential [$Cr^{IV}(PS2)_2$] compound was also synthesized (as described in the experimental section), however its structure was not determined as a single crystal suitable for X-ray diffraction could not be obtained. Nonetheless, a CV spectrum was taken and analyzed. It was found that there was one reversible reduction peak at 939 mV. This result indicates that the Cr(IV) is reduced back to Cr(III). There is also one irreversible reduction peak at 657 mV. This could possibly indicate that the Cr(III) could further be reduced to Cr(II) although this cannot be said with certainty. The fact that the $E_{1/2}$ of the oxidation of Cr(III) varies greatly from the $E_{1/2}$ of the reduction of Cr(IV) raises some questions. It could be that the desired Cr(IV) complex has *trans* phosphorus atoms. Or it could simply be that the desired Cr(IV) complex was not isolated and it is an entirely unknown complex. Regardless, a crystal structure is needed to elucidate what is occurring here. Interestingly enough the Cr(IV) complex has no peaks in the UV-VIS spectrum. This was unexpected as metal complexes traditionally do have peaks in this region corresponding to a metal to ligand charge transfer. This fact supports the idea that the desired [$Cr^{IV}(PS2)_2$] was not synthesized.

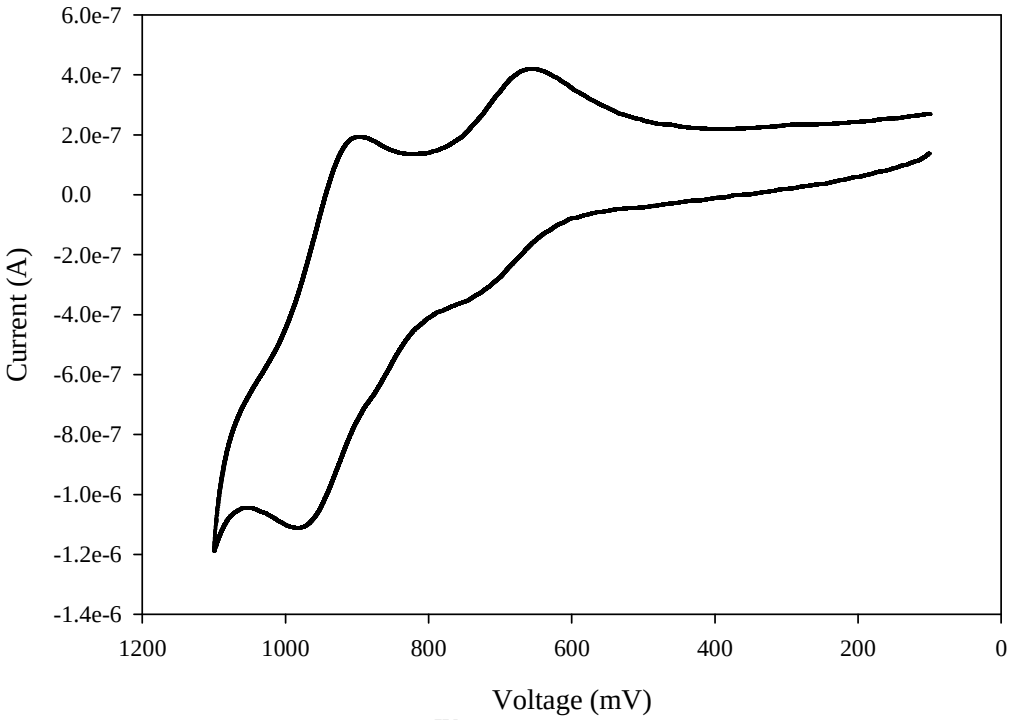

Figure 22: CV spectrum of "$[Cr^{IV}(PS2)_2]$".

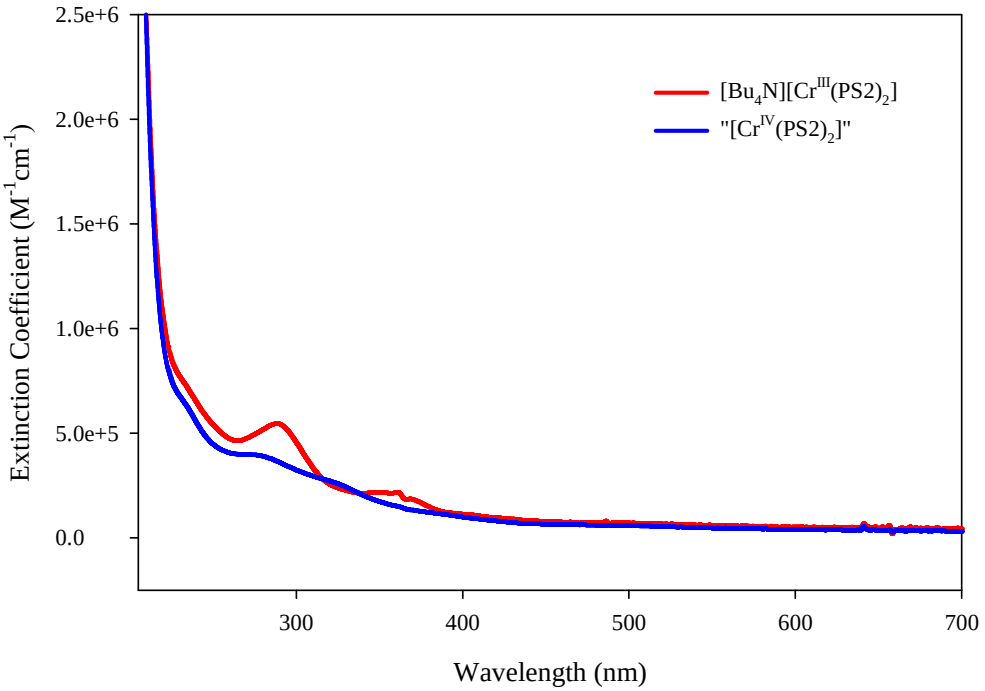

Figure 23: UV-VIS spectra of selected chromium complexes (0.1 mm path length)

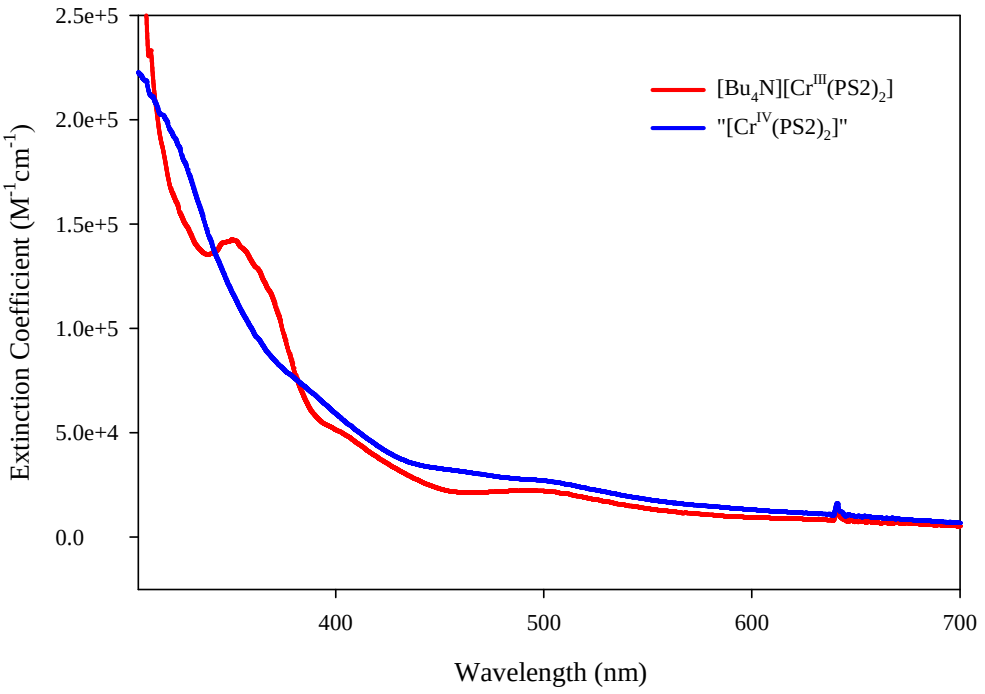

Figure 24: UV-VIS spectra of selected chromium complexes (1.0 mm path length)

Molybdenum Complexes:

Previously, a potential [$Mo^{IV}(PS2)_2$] complex was synthesized, however no crystal structure was reported for this complex[32]. In this work a [Pr_4N][$Mo^{III}(PS2)_2$] and [$Mo^{IV}(PS2)_2$] complex were synthesized successfully and a crystal structure was attempted to be determined. However, the crystals grown of each complex were not sufficient to determine the precise bond lengths and angles of each X-ray structure. This was so because the structures determined had high error values. The only conclusion that could be made from each structure was the connectivity of atoms around the metal center. For this reason the bond lengths and angles are not reported. Structurally, the complexes are very similar to the ones reported above. Both phosphorus atoms are *cis* to one another in a distorted octahedral geometry.

Electrochemically, these complexes exhibit the similar peculiar nature as observed for the complexes above. Namely the voltages reversible oxidation peak for Mo(III) and the reversible reduction peak of Mo(IV) do not equal each other as would be expected. The Mo(III) complex has an $E_{1/2}$ of 4 mV while the Mo(IV) complex has an $E_{1/2}$ of 184 mV. This observation can be explained in the same manner as above. The molybdenum complex formed electrochemically is a different isomer than what is formed synthetically.

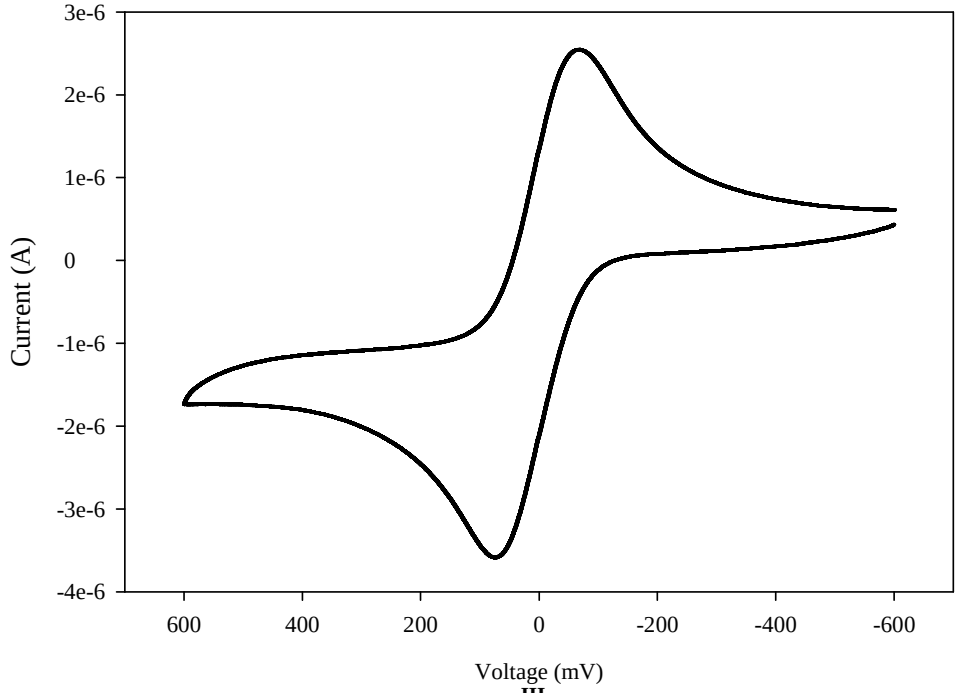

Figure 25: CV spectrum of $[Pr_4N][Mo^{III}(PS2)_2]$.

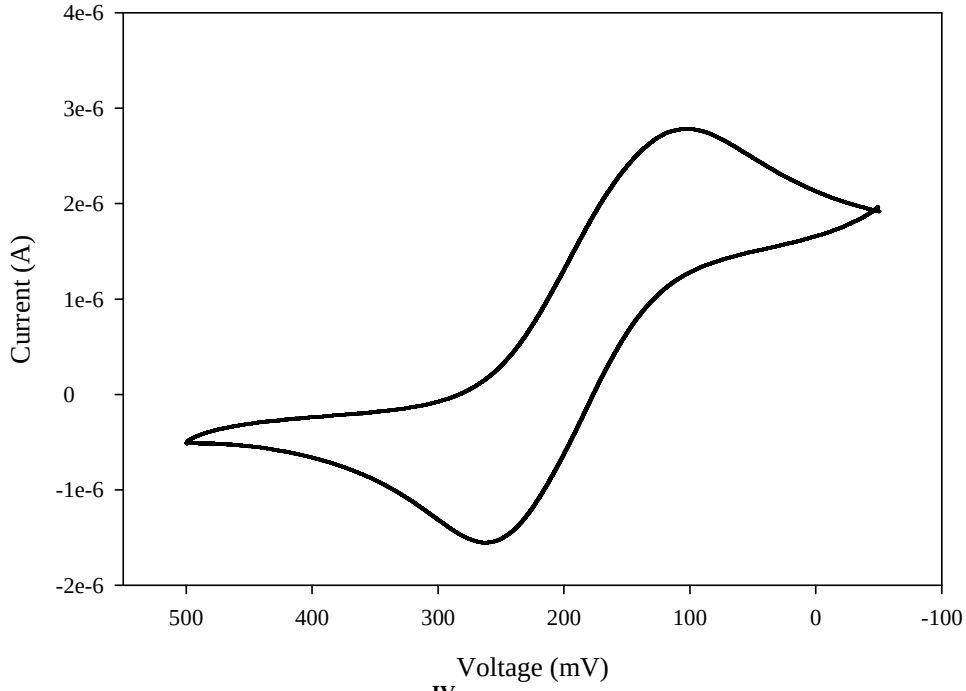

Figure 26: CV spectrum of $[Mo^{IV}(PS2)_2]$.

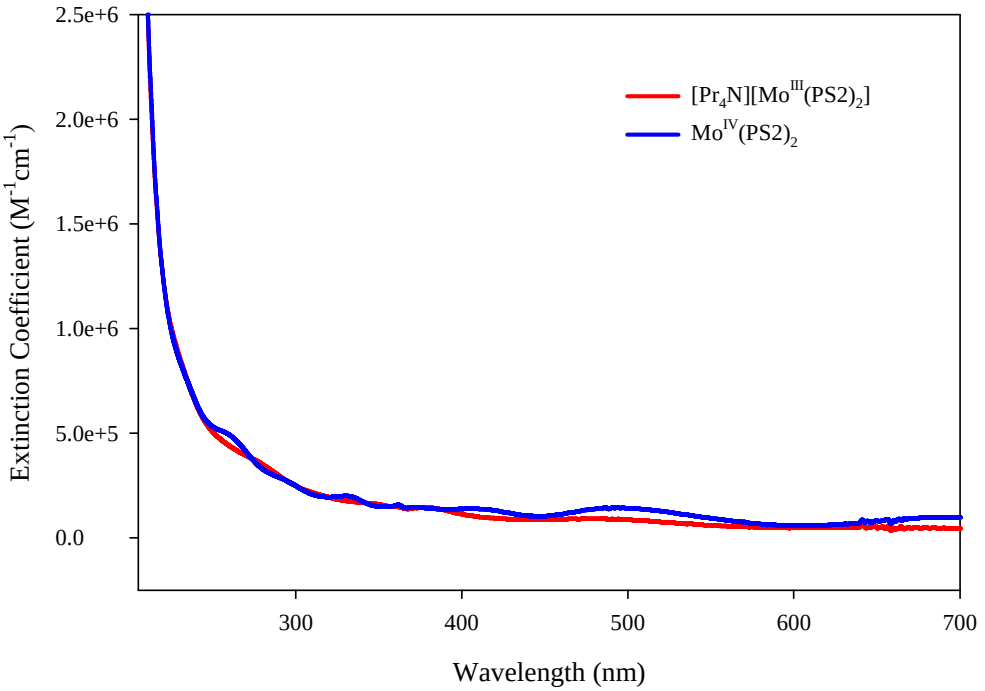

Figure 27: UV-VIS spectra of the molybdenum complexes (0.1 mm path length)

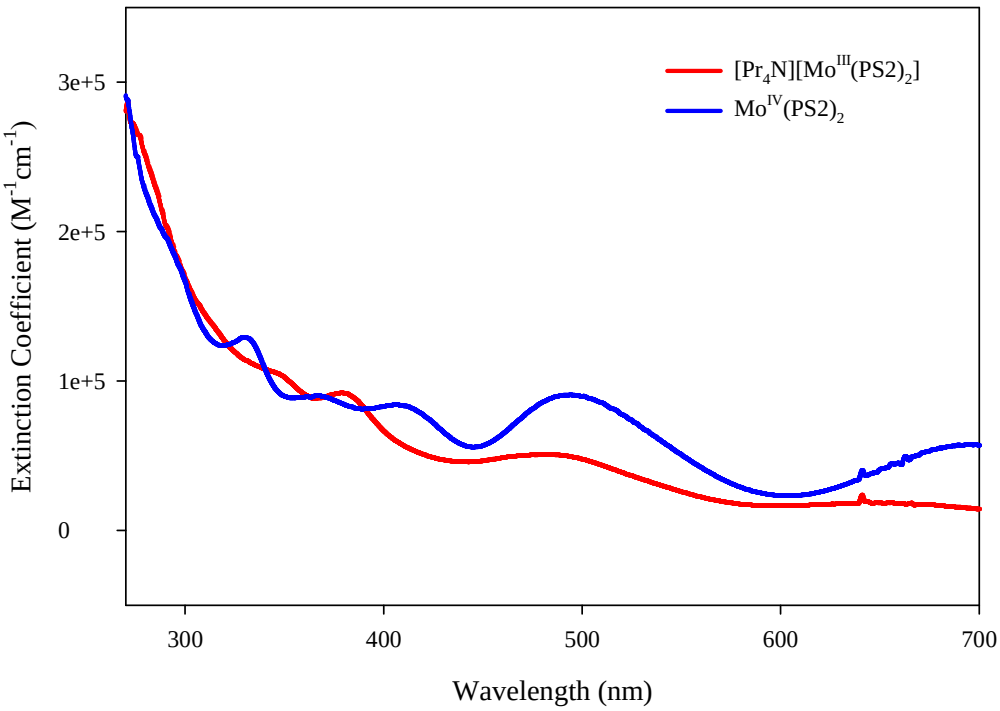

Figure 28: UV-VIS spectra of the molybdenum complexes (1.0 mm path length)

Conclusions and Future Work

Several metal complexes with the formula $[M(PS2)_2]^n$ (where n = 0 or -1) were synthesized. It was observed that these complexes exhibited the ability to be reversibly oxidized or reduced. All of these complexes had a six-coordinate distorted octahedral geometry with the phosphorus binding atoms *cis* to one another.

It is interesting to note the fact that the metal complexes that were synthesized are all stable in the high oxidation states of +3 and +4. Such metal-sulfur complexes with the metal in high formal oxidation states are rare because with the high-valent metal (+n) – thiolate centers are prone to undergo an autoredox reaction in which the sulfur atoms of the thiolate ligand (RS^-) becomes oxidized to disulfides at the same time the metal centers are reduced to a lower oxidation state (+n-1).

The CV of these compounds was not as expected. It was anticipated that the $E_{1/2}$ of complexes with identical structures but different oxidation state would be the exhibit the same $E_{1/2}$. Possibly, the redox process at the Pt working electrode is not reversible at the scan rate used. This aspects needs to be reinvestigated. Additional experiments need to be conducted to provide evidence that this is fact. Namely, CV scans can be done at different rates to see if the scan rates have an effect on the $E_{1/2}$.

Further work needs to be done to isolate and determine the structure of $[Cr^{IV}(PS2)_2]$. A better crystal of both $[Pr_4N][Mo^{III}(PS2)_2]$ and $[Mo^{IV}(PS2)_2]$ needs to be grown so the bond lengths and angles of each complex could be analyzed. Finally, work can be done with the characterized complexes to see if they have the ability to catalytically convert two protons and two electrons to dihydrogen. As with the cases of

Fe(II) and Co(II), it would be very interesting to see if the reaction of Cr(II) with two equivalents of [PS2] yields $[Cr^{III}(PS2)_2]^-$ and a half of an equivalent of H_2.

References:

1. Alper, J., Water splitting goes au naturel. *Science* **2003,** *299* (5613), 1686-1687.

2. Wilson, A. D.; Newell, R. H.; McNevin, M. J.; Muckerman, J. T.; DuBois, M. R.; DuBois, D. L., Hydrogen oxidation and production using nickel-based molecular catalysts with positioned proton relays. *J. Am. Chem. Soc.* **2006,** *128* (1), 358-366.

3. Gordon, R. B.; Bertram, M.; Graedel, T. E., Metal stocks and sustainability. *Proc. Natl. Acad. Sci. U. S. A.* **2006,** *103* (5), 1209-1214.

4. Hu, X. L.; Cossairt, B. M.; Brunschwig, B. S.; Lewis, N. S.; Peters, J. C., Electrocatalytic hydrogen evolution by cobalt difluoroboryl-diglyoximate complexes. *Chem. Commun.* **2005,** (37), 4723-4725.

5. Shima, S.; Pilak, O.; Vogt, S.; Schick, M.; Stagni, M. S.; Meyer-Klaucke, W.; Warkentin, E.; Thauer, R. K.; Ermler, U., The crystal structure of Fe -hydrogenase reveals the geometry of the active site. *Science* **2008,** *321* (5888), 572-575.

6. Block, E.; Oforiokai, G.; Zubieta, J., 2-Phosphinobenzenethiols And 2-Phosphinylbenzenethiols - New Ligand Types. *J. Am. Chem. Soc.* **1989,** *111* (6), 2327-2329.

7. Dilworth, J. R.; Wheatley, N., The preparation and coordination chemistry of phosphorus-sulfur donor ligands. *Coord. Chem. Rev.* **2000,** *199*, 89-158.

8. Figuly, G. D.; Loop, C. K.; Martin, J. C., Directed Ortho-Lithiation Of Lithium Thiophenolate - New Methodology For The Preparation Of Ortho-Substituted Thiophenols And Related-Compounds. *J. Am. Chem. Soc.* **1989,** *111* (2), 654-658.

9. Valean, A. M.; Gomez-Ruiz, S.; Lonnecke, P.; Silaghi-Dumitrescu, I.; Silaghi-Dumitrescu, L.; Hey-Hawkins, E., Stabilisation of an inorganic digallane by the phosphinobisthiolato P,S,S pincer ligand PPh(2-SC6H4)(2). *New J. Chem.* **2009,** *33* (8), 1771-1779.

10. Perez-Lourido, P.; Romero, J.; Rodriguez, L.; Garcia-Vazquez, J. A.; Castro, J.; Sousa, A.; Dilworth, J. R.; Nascimento, O. R., Synthesis, structure and characterisation of a Mn(IV) complex with a potentially tridentate phosphinothiol ligand. *Inorg. Chem. Commun.* **2002,** *5* (5), 337-339.

11. Hsu, H. F.; Su, C. L.; Gopal, N. O.; Wu, C. C.; Chu, W. C.; Tsai, Y. F.; Chang, Y. H.; Liu, Y. H.; Kuo, T. S.; Ke, S. C., Redox chemistry in the reaction of oxovanadium(V) with thiolate-containing ligands: The isolation and characterization of non-oxo vanadium(IV) complexes containing disulfide and thioether groups. *Eur. J. Inorg. Chem.* **2006,** (6), 1161-1167.

12. Hildebrand, A.; Lonnecke, P.; Silaghi-Dumitrescu, L.; Hey-Hawkins, E., Tungsten phosphanylarylthiolato complexes W{PhP(2-SC6H4)(2)-kappa S-3,S ',P}(2) and W{P(2-SC6H4)(3)-kappa S-4,S ',S ",P}(2) : Synthesis, structures and redox chemistry. *Dalton Trans.* **2008,** (34), 4639-4646.

13. Ye, S. F.; Neese, F.; Ozarowski, A.; Smirnov, D.; Krzystek, J.; Telser, J.; Liao, J. H.; Hung, C. H.; Chu, W. C.; Tsai, Y. F.; Wang, R. C.; Chen, K. Y.; Hsu, H. F., Family of V(III)-Tristhiolato Complexes Relevant to Functional Models of Vanadium Nitrogenase: Synthesis and Electronic Structure Investigations by Means of High-Frequency and -Field Electron Paramagnetic Resonance Coupled to Quantum Chemical Computations. *Inorg. Chem.* **2010,** *49* (3), 977-988.

14. Telser, J.; Wu, C. C.; Chen, K. Y.; Hsu, H. F.; Smirnov, D.; Ozarowski, A.; Krzystek, J., Aminocarboxylate complexes of vanadium(III): Electronic structure investigation by high-frequency and -field electron paramagnetic resonance spectroscopy. *J. Inorg. Biochem.* **2009,** *103* (4), 487-495.

15. Tsai, Y. F.; Huang, G. S.; Yang, C. I.; Tsai, H. L.; Liu, Y. H.; Kuo, T. S.; Hsu, H. F., Dinuclear oxovanadium(IV) thiolate complexes with ferromagnetically coupled interaction between vanadium centers. *Inorg. Chem.* **2007,** *46* (25), 10467-10469.

16. Hsu, H. F.; Peng, W. Y.; Li, Z. Y.; Wu, R. R.; Liao, J. H.; Wang, Y.; Liu, Y. H.; Shieh, M. S.; Kuo, T. S., Synthesis and structural characterization of dimolybdenum(IV) and molybdenum(VI) complexes with trisbenzenethiolatophosphine ligands. *Inorg. Chim. Acta* **2005,** *358* (6), 2149-2154.

17. Hsu, H. F.; Chu, W. C.; Hung, C. H.; Liao, J. H., The first example of a seven-coordinate Vanadium(III) thiolate complex containing the hydrazine molecule, an intermediate of nitrogen fixation. *Inorg. Chem.* **2003,** *42* (23), 7369-7371.

18. Manzer, L. E., Tetrahydrofuran Complexes of Selected Early Transition Metals. *Inorganic Syntheses* **1982,** *21*, 135-140.

19. Vanino, S., *Handbook of Preparative Chemistry* **1925**, 710.

20. Stoffelbach, F.; Saurenz, D.; Poli, R., Improved preparations of molybdenum coordination compounds from tetrachlorobis(diethyl ether)molybdenum(IV). *Eur. J. Inorg. Chem.* **2001,** (10), 2699-2703.

21. Moy, J. Transition Metal Complexes of 1,2-cyclohexanedithiolate and 2,4,6-triisopropylbenzeneselenate as Models for Metalloproteins. Stony Brook University, Stony Brook, 1991.

22. Millar, M.; Koch, S. A.; Fikar, R., The Reaction Of Fe(III) With Sterically Hindered Thiolate Ligands. *Inorganica Chimica Acta-Articles and Letters* **1984,** *88* (2), L15-L16.

23. Millar, M.; Lee, J. F.; Osullivan, T.; Koch, S. A.; Fikar, R., Models for the iron-sulfur protein rubredoxin: The use of sterically hindered thiolate ligands to stabilize Fe(SR)(4) (1-) complexes: Some considerations of the structure of the Fe(S-Cys)(4) centers in oxidized rubredoxins. *Inorg. Chim. Acta* **1996,** *243* (1-2), 333-343.

24. Osullivan, T.; Millar, M. M., Synthesis And Study Of An Analog For The Fe4S4 3+ Center Of Oxidized High-Potential Iron-Sulfur Proteins. *J. Am. Chem. Soc.* **1985,** *107* (13), 4096-4097.

25. Millar, M.; Lee, J. F.; Koch, S. A.; Fikar, R., Synthetic Models For The Iron Sulfur Protein Rubredoxin - Synthesis, Structure, And Properties Of A Highly Symmetric Iron(III) Tetrathiolate Anion. *Inorg. Chem.* **1982,** *21* (11), 4105-4106.

26. Koch, S. A.; Millar, M., Ruthenium And Osmium Thiolate Compounds. *J. Am. Chem. Soc.* **1983,** *105* (10), 3362-3363.

27. Soong, S. L.; Hain, J. H.; Millar, M.; Koch, S. A., Nitrosyl Displacement-Reactions, C-H Activation, And M-H-C Interactions In Ruthenium Thiolate Compounds. *Organometallics* **1988,** *7* (2), 556-557.

28. Satsangee, S. P.; Hain, J. H.; Cooper, P. T.; Koch, S. A., M(SR)3L2 Complexes Of Ruthenium(IV, III) And Osmium(IV) - Structural Integrity Of The Trigonal M(SR)3 +,0 Cores. *Inorg. Chem.* **1992,** *31* (25), 5160-5161.

29. Millar, M. M.; Osullivan, T.; Devries, N.; Koch, S. A., Ruthenium(IV) And Osmium(IV) Chalcogen Complexes Of Carbon-Monoxide. *J. Am. Chem. Soc.* **1985,** *107* (12), 3714-3715.

30. Fikar, R.; Koch, S. A.; Millar, M. M., A Square-Planar Cobalt(III) Tetrathiolate Complex. *Inorg. Chem.* **1985,** *24* (21), 3311-3312.

31. Beatty, S. Transition Metal Phosphine-Thiolate Complexes
as Models for Metalloproteins. Stony Brook University, Stony Brook, 1997.

32. Dilworth, J. R.; Hutson, A. J.; Lewis, J. S.; Miller, J. R.; Zheng, Y. F.; Chen, Q.; Zubieta, J., Complexes of potentially tri- and tetra-dentate phosphinothiol ligands with Mo, W, Re, Fe, Ru, Os, Rh, Ir and Ni. *J. Chem. Soc.-Dalton Trans.* **1996,** (6), 1093-1104.

Appendix

Table A-1. Crystal data and structure refinement for $[Et_4N][V^{III}(PS2)_2]$

Empirical formula	C44 H46 N P2 S4 V	
Formula weight	829.94	
Temperature	293(2) K	
Wavelength	0.71073 Å	
Crystal system	Monoclinic	
Space group	$P2_1/c$	
Unit cell dimensions	a = 16.29546(20) Å	α= 90°.
	b = 13.81839(15) Å	β= 92.4605(11)°.
	c = 18.0290(2) Å	γ = 90°.
Volume	4055.98(8) $Å^3$	
Z	4	
Density (calculated)	1.359 Mg/m^3	
Absorption coefficient	0.562 mm^{-1}	
F(000)	1736	
Crystal size	0.4 x 0.3 x 0.2 mm^3	
Theta range for data collection	3.20 to 29.60°.	
Index ranges	-15<=h<=22, -18<=k<=18, -22<=l<=24	
Reflections collected	22152	
Independent reflections	9763 [R(int) = 0.0222]	
Completeness to theta = 29.60°	85.5 %	
Refinement method	Full-matrix least-squares on F^2	
Data / restraints / parameters	9763 / 0 / 469	
Goodness-of-fit on F^2	0.973	
Final R indices [I>2sigma(I)]	R1 = 0.0274, wR2 = 0.0622	
R indices (all data)	R1 = 0.0430, wR2 = 0.0642	
Largest diff. peak and hole	0.380 and -0.274 $e.Å^{-3}$	

Table A-2. Crystal data and structure refinement for $[Et_4N][V^{III}(POS2)_2]$

Empirical formula	C184 H200 Cl16 N4 O8 P8 S16 V4	
Formula weight	4127.16	
Temperature	293(2) K	
Wavelength	0.71073 Å	
Crystal system	Monoclinic	
Space group	$P2_1/n$	
Unit cell dimensions	a = 20.2103(15) Å	α= 90°.
	b = 11.1589(5) Å	β= 111.642(8)°.
	c = 23.0585(15) Å	γ = 90°.
Volume	4833.7(5) $Å^3$	
Z	4	
Density (calculated)	1.418 Mg/m^3	
Absorption coefficient	0.704 mm^{-1}	
F(000)	2136	
Crystal size	0.5 x 0.2 x 0.05 mm^3	
Theta range for data collection	3.22 to 21.75°.	
Index ranges	-20<=h<=21, -11<=k<=11, -22<=l<=24	
Reflections collected	16824	
Independent reflections	5705 [R(int) = 0.0737]	
Completeness to theta = 21.75°	99.3 %	
Refinement method	Full-matrix least-squares on F^2	
Data / restraints / parameters	5705 / 0 / 541	
Goodness-of-fit on F^2	0.788	
Final R indices [I>2sigma(I)]	R1 = 0.0390, wR2 = 0.0692	
R indices (all data)	R1 = 0.0831, wR2 = 0.0747	
Largest diff. peak and hole	0.614 and -0.482 $e.Å^{-3}$	

Table A-3. Crystal data and structure refinement for $V^{IV}(PS2)_2$

Empirical formula	C36 H26 P2 S4 V	
Formula weight	699.69	
Temperature	293(2) K	
Wavelength	0.71073 Å	
Crystal system	Orthorhombic	
Space group	$P2_12_12_1$	
Unit cell dimensions	a = 12.4885(3) Å	α= 90°.
	b = 12.7287(3) Å	β= 90°.
	c = 20.0915(4) Å	γ = 90°.
Volume	3193.79(12) $Å^3$	
Z	4	
Density (calculated)	1.455 Mg/m^3	
Absorption coefficient	0.699 mm^{-1}	
F(000)	1436	
Crystal size	1.0 x 0.20 x 0.2 mm^3	
Theta range for data collection	3.36 to 32.81°.	
Index ranges	-17<=h<=14, -14<=k<=18, -19<=l<=30	
Reflections collected	15106	
Independent reflections	10068 [R(int) = 0.0233]	
Completeness to theta = 32.81°	91.5 %	
Refinement method	Full-matrix least-squares on F^2	
Data / restraints / parameters	10068 / 0 / 388	
Goodness-of-fit on F^2	0.978	
Final R indices [I>2sigma(I)]	R1 = 0.0325, wR2 = 0.0638	
R indices (all data)	R1 = 0.0463, wR2 = 0.0664	
Absolute structure parameter	0.018(15)	
Largest diff. peak and hole	0.434 and -0.355 e.$Å^{-3}$	

Table A-4. Crystal data and structure refinement for $[Bu_4N][Cr^{III}(PS2)_2]$.

Empirical formula	C104 H124 Cr2 N2 P4 S8	
Formula weight	1886.41	
Temperature	293(2) K	
Wavelength	0.71073 Å	
Crystal system	Tetragonal	
Space group	*P*-4	
Unit cell dimensions	a = 31.0727(5) Å	α= 90°.
	b = 31.0727(5) Å	β= 90°.
	c = 10.2498(3) Å	γ = 90°.
Volume	9896.3(4) $Å^3$	
Z	4	
Density (calculated)	1.266 Mg/m^3	
Absorption coefficient	0.500 mm^{-1}	
F(000)	3992	
Crystal size	0.4 x 0.3 x 0.3 mm^3	
Theta range for data collection	3.28 to 32.89°.	
Index ranges	-45<=h<=26, -40<=k<=35, -15<=l<=14	
Reflections collected	39172	
Independent reflections	29879 [R(int) = 0.0345]	
Completeness to theta = 32.89°	89.7 %	
Refinement method	Full-matrix least-squares on F^2	
Data / restraints / parameters	29879 / 0 / 1081	
Goodness-of-fit on F^2	0.989	
Final R indices [I>2sigma(I)]	R1 = 0.0656, wR2 = 0.1405	
R indices (all data)	R1 = 0.1033, wR2 = 0.1486	
Absolute structure parameter	0.928(18)	
Largest diff. peak and hole	0.771 and -0.756 e.$Å^{-3}$	

Table A-5. Crystal data and structure refinement for $[Bu_4N][Cr^{III}(PS2')_2]$

Empirical formula	C56 H70 Cr N P2 S4	
Formula weight	999.31	
Temperature	293(2) K	
Wavelength	0.71073 Å	
Crystal system	Monoclinic	
Space group	$P2_1$	
Unit cell dimensions	a = 16.3014(3) Å	α= 90°.
	b = 15.8573(2) Å	β= 95.817(2)°.
	c = 21.1419(4) Å	γ = 90°.
Volume	5436.93(18) $Å^3$	
Z	4	
Density (calculated)	1.221 Mg/m^3	
Absorption coefficient	0.459 mm^{-1}	
F(000)	2124	
Crystal size	0.8 x 0.5 x 0.1 mm^3	
Theta range for data collection	2.86 to 35.09°.	
Index ranges	-23<=h<=26, -24<=k<=25, -33<=l<=33	
Reflections collected	67486	
Independent reflections	38925 [R(int) = 0.0739]	
Completeness to theta = 35.09°	92.0 %	
Refinement method	Full-matrix least-squares on F^2	
Data / restraints / parameters	38925 / 1 / 1153	
Goodness-of-fit on F^2	0.904	
Final R indices [I>2sigma(I)]	R1 = 0.0645, wR2 = 0.1558	
R indices (all data)	R1 = 0.1579, wR2 = 0.1685	
Absolute structure parameter	-0.019(19)	
Largest diff. peak and hole	2.990 and -0.607 $e.Å^{-3}$	

Table A-6. Crystal data and structure refinement for $[Et_4N][Mn^{III}(PS2')_2]$

Empirical formula	C48 H54 Mn N P2 S4	
Formula weight	890.04	
Temperature	293(2) K	
Wavelength	0.71073 Å	
Crystal system	Triclinic	
Space group	*P*-1	
Unit cell dimensions	a = 9.6875(2) Å	α= 82.286(2)°.
	b = 13.7174(4) Å	β= 84.549(2)°.
	c = 18.1469(5) Å	γ = 86.132(2)°.
Volume	2375.20(12) $Å^3$	
Z	2	
Density (calculated)	1.244 Mg/m^3	
Absorption coefficient	0.553 mm^{-1}	
F(000)	936	
Crystal size	0.4 x 0.2 x 0.2 mm^3	
Theta range for data collection	2.88 to 29.56°.	
Index ranges	-13<=h<=13, -18<=k<=18, -24<=l<=23	
Reflections collected	39064	
Independent reflections	11590 [R(int) = 0.0490]	
Completeness to theta = 29.56°	87.0 %	
Refinement method	Full-matrix least-squares on F^2	
Data / restraints / parameters	11590 / 0 / 505	
Goodness-of-fit on F^2	2.164	
Final R indices [I>2sigma(I)]	R1 = 0.0956, wR2 = 0.2805	
R indices (all data)	R1 = 0.1229, wR2 = 0.2894	
Largest diff. peak and hole	4.885 and -0.436 e.$Å^{-3}$	

Table A-7. Crystal data and structure refinement for $Mn^{IV}(PS2')_2$

Empirical formula	C40 H34 Mn P2 S4	
Formula weight	759.79	
Temperature	293(2) K	
Wavelength	0.71073 Å	
Crystal system	Monoclinic	
Space group	$P2_1/c$	
Unit cell dimensions	a = 14.975(2) Å	α= 90°.
	b = 15.309(2) Å	β= 90.94(3)°.
	c = 17.919(3) Å	γ = 90°.
Volume	4107.4(2) $Å^3$	
Z	4	
Density (calculated)	1.229 Mg/m^3	
Absorption coefficient	0.628 mm^{-1}	
F(000)	1572	
Crystal size	1.0 x 0.8 x 0.1 mm^3	
Theta range for data collection	1.36 to 28.22°.	
Index ranges	-19<=h<=17, -9<=k<=17, -23<=l<=22	
Reflections collected	16227	
Independent reflections	8120 [R(int) = 0.0727]	
Completeness to theta = 28.22°	80.1 %	
Refinement method	Full-matrix least-squares on F^2	
Data / restraints / parameters	8120 / 0 / 440	
Goodness-of-fit on F^2	0.897	
Final R indices [I>2sigma(I)]	R1 = 0.0760, wR2 = 0.2221	
R indices (all data)	R1 = 0.1496, wR2 = 0.3046	
Largest diff. peak and hole	1.644 and -0.812 $e.Å^{-3}$	